Received: 28 May 2019 | Revised: 8 April 2020 | Accepted: 8 April 2020

DOI: 10.1002/dep2.116

ORIGINAL RESEARCH ARTICLE

The Depositional Record Open Access
A journal of the International Association of Sedimentologists
WILEY

Dynamic of a lacustrine sedimentary system during late rifting at the Cretaceous–Palaeocene transition: Example of the Yacoraite Formation, Salta Basin, Argentina

Rémy Deschamps[1] | **Sébastien Rohais**[1] | **Youri Hamon**[1] | **Marta Gasparrini**[1,2]

[1]IFPEN, Rueil Malmaison, France

[2]Earth Sciences Department, University of Milan, Milan, Italy

Correspondence
Rémy Deschamps, IFPEN, 1-4 avenue bois préau, 92852 Rueil Malmaison, France.
Email: remy.deschamps@ifpen.fr

Abstract

The architecture of lacustrine systems is the result of the complex interaction between tectonics, climate and environmental parameters, and constitute the main forcing parameters on the lake dynamics. Field analogue studies have been performed to better assess such interactions, and their impact on the facies distribution and the stratigraphic architecture of lacustrine systems. The Yacoraite Formation (Late Cretaceous/Early Palaeocene), deposited during the sag phase of the Salta rift basin in Argentina, is exposed in world-class outcrops that allowed the dynamics of this lacustrine system to be studied through facies analysis and stratigraphic evolution. On the scale of the Alemania-Metán-El Rey Basin, the Yacoraite Formation is organized with a siliciclastic-dominated margin to the west, and a carbonate-dominated margin to the east. The Yacoraite can be subdivided into four main 'mid-term' sequences and further subdivided into 'short-term' sequences recording high frequency climate fluctuations. Furthermore, the depositional profiles and identified system tracts have been grouped into two end-members at basin scale: (a) a balanced 'perennial' depositional system for the lower part of the Yacoraite Formation and (b) a highly alternating 'ephemeral' depositional system for the upper part of the Yacoraite Formation. The transition from a perennial system to an ephemeral system indicates a change in the sedimentary dynamics of the basin, which was probably linked with the Cretaceous/Tertiary boundary that induced a temporary shutdown of carbonate production and an increase in siliciclastic supply.

KEYWORDS

Cretaceous/Tertiary, lacustrine, rift basin, sedimentary, Yacoraite Formation

1 | INTRODUCTION

Interest in lacustrine systems has increased worldwide over the last few decades due to recent hydrocarbon discoveries in the South Atlantic pre-salt Cretaceous lacustrine series (Rangel and Carminatti, 2000; Gomes *et al.*, 2009), and also following acquisition of accurate records of the various factors controlling the stratigraphic architecture (i.e., climate,

environmental and tectonic settings) at basin scale and at different time scales (Bohacs *et al*., 2003; Alonso Zarza and Tanner, 2008).

In rift settings, the architecture of lacustrine systems is mainly controlled by tectonics and climate (Blair and Bilodeau, 1988; De Wet *et al*., 1998; Bohacs *et al.*, 2000). The recognition of stratigraphic sequences in continental settings, and particularly in lacustrine rift settings, helps us to understand and characterize the stratigraphic architecture at basin scale, allowing the controlling factors of sequence development to be deciphered in rift basins (Shanley and McCabe, 1994; Lin *et al.*, 2001; Pietras and Carrol, 2006). During rifting processes, the subsidence pattern evolves from starved and underfilled basins during the tectonic subsidence phase, towards overfilled basins surrounded by topographic highs during the decay phase of tectonic subsidence and the onset of thermal subsidence (Picarelli and Abreu, 2012). In stable subsiding rift systems (i.e., thermal sag phase), climate variations strongly overprint the tectonic effect on stratigraphic architecture, the nature of the facies, and their distribution within the basin (Cloething *et al.*, 1985; Seranne and Anka, 2005; Scherer *et al.*, 2015). The subsidence pattern during the sag phase is more homogeneous throughout the basin, and lacustrine deposition controlled by climate changes becomes predominant (Lambiase and Bosworth, 1995; Contreras *et al.*, 1997).

The Yacoraite Formation is a lacustrine system deposited in the Salta rift basin (NW Argentina, Figure 1), during the sag phase of the rifting, and is dated Upper Cretaceous to Lower Palaeocene (Reyes, 1972; Salfity, 1982; Marquillas *et al.*, 2007; Rohais *et al.*, 2019). The Yacoraite Formation crops out in the Alemania-Metán-El Rey sub-basins (Figure 2). The quality of the Yacoraite Formation exposures in various locations of the Alemania-Metán sub-basin (Bento Freire, 2012; Roemers *et al.*, 2015; Bunevich *et al.*, 2017) permitted the stratigraphic architecture of this formation to be reconstructed. The Yacoraite Formation is partitioned into a clastic-dominated margin to the west and a carbonate-dominated margin to the east. Sequential analysis and system tracts definition made it possible to assess the vertical and lateral variability of the Yacoraite Formation depositional architecture, and thus to understand the evolution of the lake dynamic through variations in factors such as climate and tectonics, that control sediment supply. The Yacoraite Formation spans the Cretaceous–Tertiary boundary (K–T) and as the K–T event strongly impacted the climate (Kring, 2003; Ocampo *et al.*, 2006; Schulte, 2010; Vellekoop *et al.*, 2014, Rohais *et al.*, 2019) a drastic change in the sedimentation pattern can be expected within the Yacoraite lacustrine system. Rohais *et al.* (2019) studied the same stratigraphic interval in the Salta Basin. They used multi-proxy analysis to evaluate the source rock potential and evolution of the organic–rich lacustrine deposits through the K–T event, characterized by rapid and drastic change in climate. Consequently, the climate change at the K–T boundary affected the sedimentary deposits, with variations in the supply of sediment to the basin having a strong impact on the distribution and quality of the organic matter (Rohais *et al.*, 2019).

The first objective of this paper is to analyze the dynamics of a lacustrine system over its complete life cycle, which was set up during the early sag phase of a rift system and ended

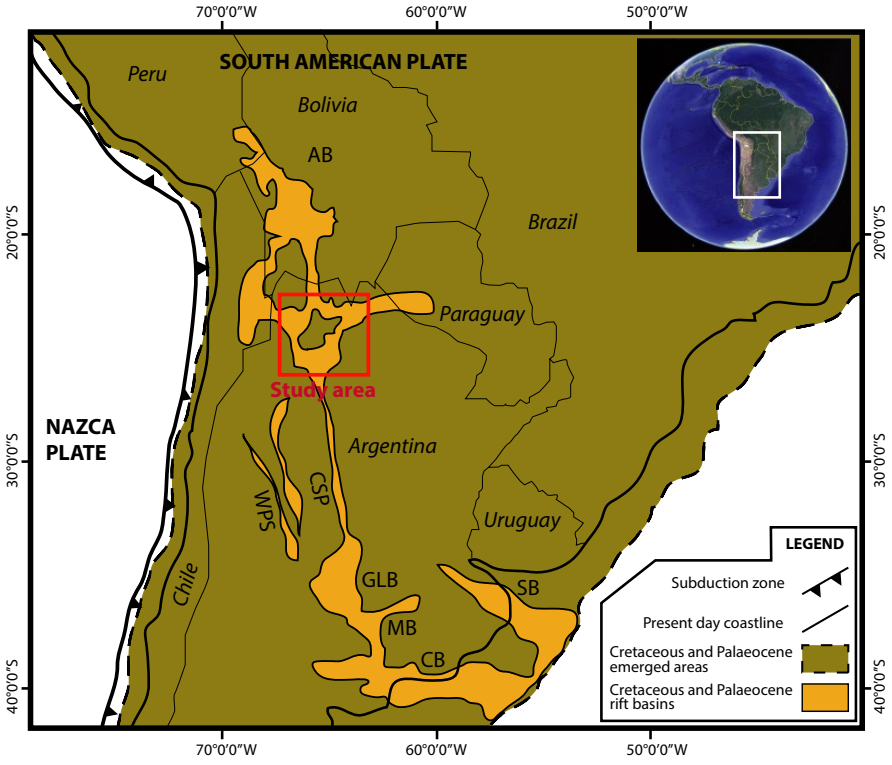

FIGURE 1 Map showing the location of Cretaceous and Palaeocene rift basins of Southern America (modified from Uliana *et al.*, 1989). Abbreviations are RB, Rawson Basin; CB, Colorado Basin; SB, Salado Basin; MB, Mascachin Basin; GLB, General Lavalle Basin; WPS, Western Pampean Basin; CPS, Central Pampean Basin; AB, Andean Basin

during a late rifting phase (onset of the post-rift phase). The lake dynamic is unravelled through a detailed facies analysis that helps to reconstruct the stratigraphic architecture of the Yacoraite Formation in the Alemania- Metán sub-basins, and thus decipher the main factors that controlled deposition.

The second objective of this work is to analyze and understand how a lacustrine depositional system reacts to a major forcing. The K–T transition within the Yacoraite Formation was examined with the intent of analyzing the effect of the K–T climate change on the sedimentation record at basin scale, and the consequences of this on the basin dynamic and on the stratigraphic architecture.

2 | GEOLOGICAL SETTING OF THE SALTA RIFT BASIN

The Salta rift basin is part of the Cretaceous-Palaeocene Andean basin system of central-western South America (Figure 1). This basin was initially interpreted as an aborted foreland rift (Galliski and Viramonte, 1988) as it is commonly associated in a back-arc setting with the subduction of the Nazca Plate underneath the South American Plate. Re-interpretation of magmatic and volcanic events occurring during basin evolution suggests that the basin was probably

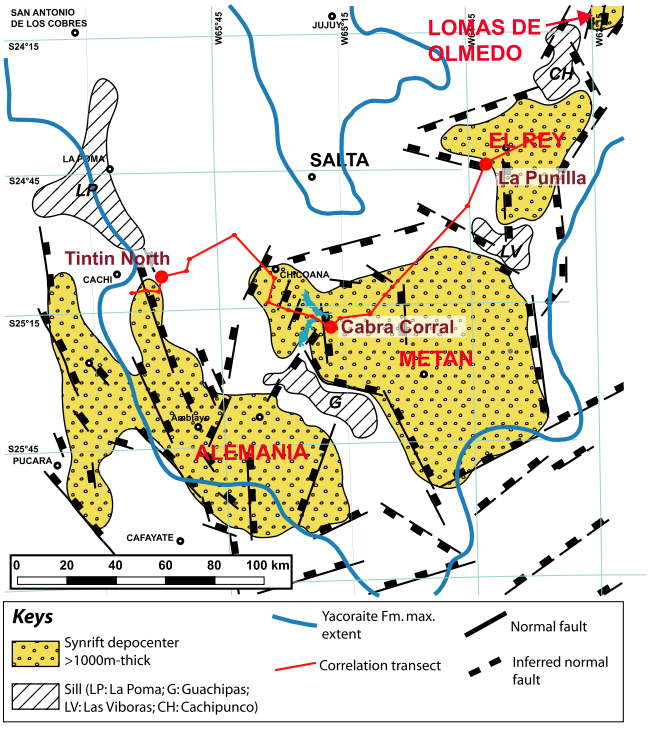

FIGURE 2 Location of the Salta rift basin and the main sub-basins within the rift identified by syn-rift depocenters >1,000 m thick (modified from Salfity, 1982; Marquillas, 1985; Cristallini *et al.*, 1998; Viramontes *et al.*, 1999; Carrera *et al.*, 2006; 2009). Sill: LP La Poma, G Guachipas, LV Las Viboras, CH Cachipunco

associated with the opening of the South Atlantic Ocean initiated during the Barremian (Viramonte *et al.*, 1999).

Several depocenters were identified during the syn-rift evolution of the Salta Basin with three main sub-basins in the study area: the El Rey, Alemania and Metán sub-basins (Figure 2). The Alemania depocenter is localized to the south-west of the city of Alemania, Argentina. The structural map presented in Figure 2 is based on Carrera *et al.* (2006; 2009) who identified several sub-depocenters within the three large syn-rift depocenters (cutoff at >1,000 m of thickness for the three larger depocenters). The Guachipas (G) palaeohigh subdivided the Alemania-Metán area with relatively thin syn-rift deposits (200–500 m thick).

The Salta rift basin fill (Figure 3) can be subdivided into three main stages: syn-rift (Pirgua Subgroup), transitional sag (Balbuena Subgroup) and post-rift (Santa Barbara Subgroup). The transitional sag has also been described as an early post-rift phase (Salfity and Marquillas, 1994).

2.1 | Syn-rift

The syn-rift phase is recorded by the Pirgua Subgroup (Reyes and Salfity, 1973). It corresponds to continental red beds (conglomerates, sandstones and siltstones) and volcanic rocks. The succession can be up to 4,000 m thick in the main depocenter and rapidly thins towards the margins of the rift. The base of the Pirgua Subgroup is well-dated (Barremian) by the interbedded volcanics of the Alto de Las Salinas Complex (Bossi, 1969), which gave ages of 128–112 Ma (K/Ar, whole rock) in the southern part of the basin (Alemania area), and also by other volcanic rocks giving ages of 126 ± 3.5 Ma (method not specified) in the Paraguayan portion of the Lomas de Olmedo sub-basin (Clebsch, 1991).

The Pirgua Subgroup is subdivided into two syn-rift cycles: the first one recorded by the La Yesera Formation, and the second one by the Las Curtiembres Formation and the Los Blanquitos Formation (Figure 3). The La Yesera Formation recorded a fining-upward cycle from alluvial fan to fluvio-braided plain and shallow lacustrine deposits. This first cycle is followed by a sharp coarsening-upward cycle (upper La Yesera Formation) composed of coarse-grained alluvial fan deposits. The upper La Yesera Formation is interbedded with the Isonza Basalt, probably of Cenomanian age (96 ± 5 to 99 ± 5 Ma, K/Ar whole rock; Valencio *et al.*, 1976).

The Las Curtiembres Formation recorded a rapid fining-upward cycle characterized by fresh to brackish lake fine-grained deposits. This formation probably recorded the rift climax. The upper part of the Las Curtiembres Formation is locally (central part of the rift) interbedded with the Las Conchas Basalt dated at 78 ± 5 Ma and 76.4 ± 3.5 Ma (K/Ar ages; Reyes *et al.*, 1976; Valencio *et al.*, 1976; Galliski and Viramonte, 1988). The Las Curtiembres

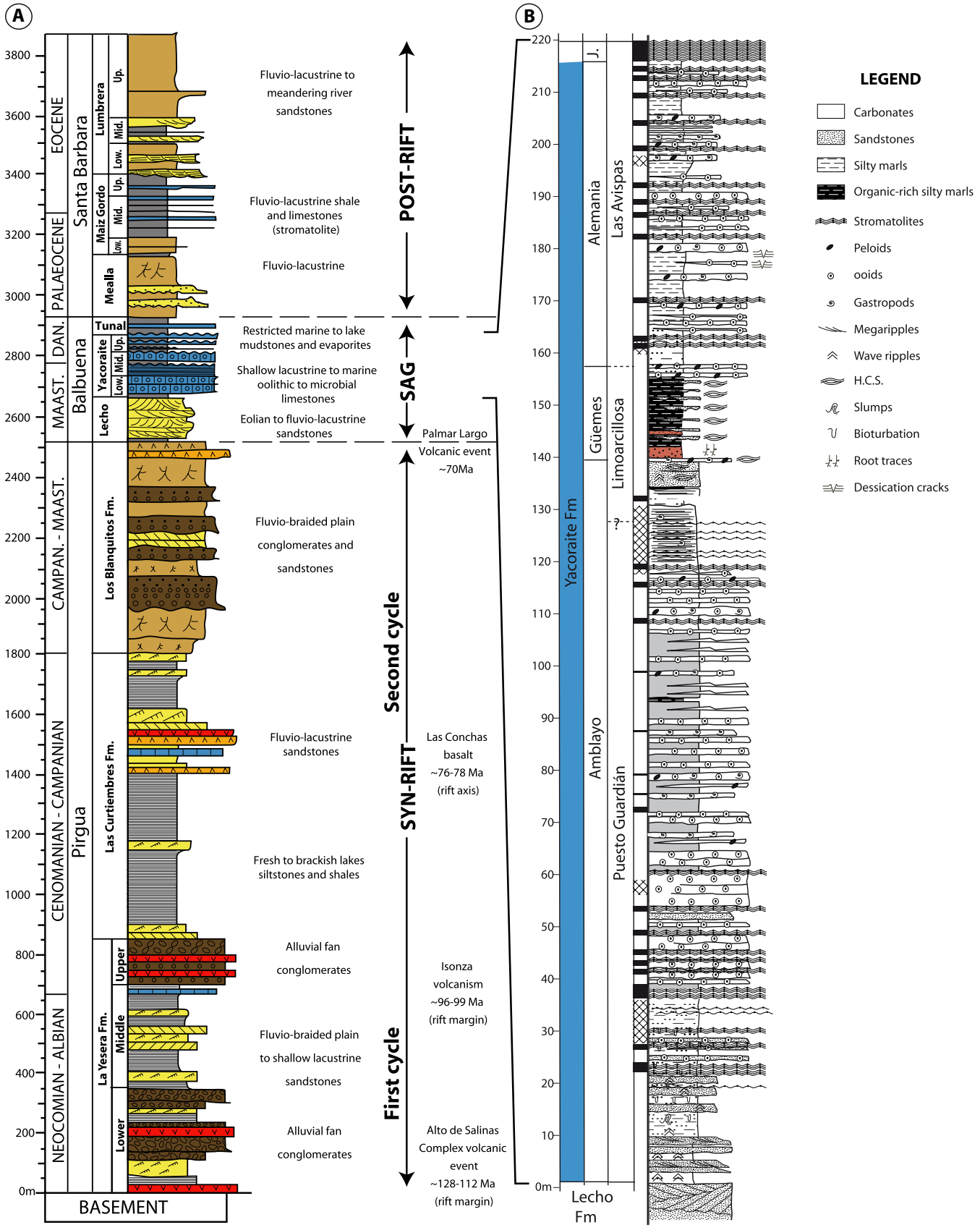

FIGURE 3 Stratigraphic section of the sedimentary fill from the Salta rift basin based on outcrop observation (modified from Marquillas *et al.*, 2005). To the left: Cabra Corral/Juramento area synthetic section

Formation progressively evolves upwards to the Los Blanquitos Formation made of fluvio-braided plain coarse-grained deposits.

The Los Blanquitos Formation is organized in a coarsening-upward cycle recording the end of the main fault activity. Fossil remains (sauropod dinosaurs; Bonaparte and Bossi, 1967) from the upper part of the Los Blanquitos Formation indicate a Senonian age (Powell, 1979). This age is fairly consistent with the Palmar Largo volcanic rocks (Mädel, 1984) interbedded between the top of the Los Blanquitos Formation and the base of the Balbuena Subgroup in the Lomas de Olmedo sub-basin (70 ± 5 Ma by K/Ar method, Early Maastrichtian; Gómez-Omil *et al*., 1987).

2.2 | Sag phase

The sag phase (initiation of thermal subsidence) is recorded by the Balbuena Subgroup (Figure 3). The latter can reach 400–500 m in thickness, and is subdivided into three formations: the Lecho Formation, the Yacoraite Formation and the Olmedo/Tunal formations (respectively subsurface and outcrop equivalent of the overlying series). The Lecho Formation corresponds to fine to coarse-grained sandstones deposited in aeolian to fluvio-lacustrine environments. It is organized in an overall transgressive trend from fluvial to aeolian deposits during the Maastrichtian.

The Yacoraite Formation (up to 220 m thick) corresponds to shales, mudstones, oolitic and stromatolitic limestones and interbedded fine-grained sandstones deposited in shallow marine to lacustrine environments. The transgressive trend initiated during the Lecho Formation deposition continued during the deposition of the Yacoraite Formation. The Yacoraite Formation can be subdivided into three main packages that correspond to the main members used to define this formation in the reference section in the Cabra Corral area (Figure 2). The Amblayo Member at the bottom, characterized by carbonate-dominated deposits; the Güemes Member, dominated by clastic deposits; and the Alemania Member, that corresponds to alternating shallow carbonate beds with marly deposits (Marquillas *et al.*, 2005). Tuff/ash layers are common. In the Lomas de Olmedo sub-basin, volcanics from the Palmar Largo event (*ca* 70 ± 5 Ma) are interbedded within the Yacoraite Formation. Lamprophyre sills intruded into the Los Blanquitos Formation have K/Ar ages of 65 and 60 ± 2 Ma (Fernandez, 1975; Omarini *et al.*, 1989). The age of the Yacoraite Formation is Maastrichtian to Danian (Marquillas, 1985), based on Senonian dinosaur tracks (Alonso and Marquillas, 1986) and Maastrichtian and Danian palynomorphs (Moroni, 1982). More recent publications (Marquillas *et al.*, 2011) based on Tuff/ash dating (U/Pb zircon) indicates ages ranging from 71.9 ± 0.4 Ma for the basal part of the Yacoraite Formation to 68.4 ± 0.7 Ma for the upper part. Timing and duration of the depositional interval for the entire Yacoraite Formation have been recently updated and adjusted to a range of 69.1 ± 0.7 Ma to 64.0 ± 0.5 Ma based on U/Pb zircon dating of eight ash layers (Rohais *et al.*, 2019). The Yacoraite Formation was deposited during a period of tectonic quiescence, as no major tectonic changes were recorded during the sag phase of the basin, supported by backstripping results on subsurface well data that confirmed no breaks in the subsidence rate (Starck, 2011).

The Olmedo/Tunal formations correspond to dark shales, halite, anhydrite and gypsum deposited in lacustrine, brackish to hypersaline lake environments that record a major change in the lacustrine dynamic toward the following main sequence boundary at the base of the Mealla Formation (Santa Barbara Subgroup). The Tunal Formation is Danian (65.5–61.7 Ma) according to its palynologic content (Quattrocchio *et al.*, 2000).

2.3 | Post-rift

The post-rift phase is recorded by the Santa Barbara Subgroup (Figure 3). It can be subdivided into three formations: the Mealla Formation, the Maiz Gordo Formation and the Lumbrera Formation (Moreno, 1970).

The Mealla Formation (up to 150 m thick) corresponds to reddish siltstones to coarse-grained sandstones deposited in fluvio-lacustrine to meandering plain environments. It laterally passes eastwards (Lomas de Olmedo sub-basin) to claystones, siltstones, gypsum and discrete stromatolites deposited in lacustrine to hypersaline lakes (Gómez-Omil *et al.*, 1987).

The Maiz Gordo Formation (up to 250 m thick) corresponds to fluvio-lacustrine fine to coarse-grained sandstones and limestones (oolite and stromatolite). Palynomorph communities and non-marine dinoflagellates indicate Thanetian ages (Quattrochio and del Papa, 2000).

The Lumbrera Formation (400–500 m thick) corresponds to fluvio-lacustrine red mudstones to coarse-grained sandstones, and sporadic gypsum/anhydrite nodules (Marquillas *et al.*, 2005).

3 | MATERIALS AND METHODS

The Yacoraite Formation crops out in several well-exposed cliffs. Twenty-seven detailed sedimentological sections, subsurface cores and mining cores were described (1:100 scale) and sampled to illustrate facies diversity. These facies descriptions were subsequently used to build stratigraphic correlations

TABLE 1 Facies description of the Yacoraite Formation

Facies	Lithology/Texture	Sedimentary structures/Bedform	Skeletal components	Non-skeletal components	Environmental interpretation
S1: Massive coarse-grained sandstones	Poorly sorted medium to very coarse-grained sandstones with centimetre-scale floating gravels	No structures, grading (fining upwards)	N/A	Floating granules in medium to coarse grained sandy matrix	Grain flow deposits/channel bars in alluvial fan
S2: Cross-bedded sandstones	Fining upwards medium to coarse-grained sandstones	Erosive based channel bedforms, trough cross-stratifications, plane parallel bedding, current ripples	N/A	Basal lags with granules, fining upwards	Fluvial channels
S3: Red silty shales and siltstones with root traces	Mottled reddish to greenish shaly siltstones with root traces	Current ripples	N/A	Root traces, white carbonate nodules, rhizoconcretions	Alluvial plain/Floodplain
S4: Steep angled cross-laminated sandstones	Badly sorted medium to coarse-grained	Sharp base, coarsening upwards, mud clasts, steep angle tabular cross-bedding	Gastropod basal lag	Floating quartz and feldspar granules, bioturbation	Prograding delta front
S5: Wave and current rippled siltstones/ sandstones	Thinly laminated well sorted siltstones to very fine grained sandstones	Wave ripples, occasional current ripples	N/A	Dessication cracks, occasional stromatolite clasts, charophytes	Sandflat
S6: Sigmoidal cross-bedded sandstones	Well sorted fine to medium-grained sandstone	Erosive base, coarsening upwards, sigmoidal cross-stratifications with mud drapes, wave ripples on top of beds	Rare bioclasts	Mud clasts, rip up clasts, bioturbation	Longshore bars/sandbars in shallow lacustrine environment
S7: Low angle cross-bedded sandstones	Well sorted medium to coarse-grained sandstone	Plane parallel to low-angle cross-bedding. Occasional wave ripples	Rare bioclasts	Rare ooids	High energy shore/Upper shoreface
S8: Wave laminated sandstones	Well sorted fine to medium-grained sandstone	Plane parallel bedding, wave ripples	Rare bioclasts	Abundant bioturbation	Low energy shore/Lower shoreface
S9: Hummocky cross-stratified sandstones	Very fine to medium-grained sandstones	Lens-shape graded beds with erosive base (Hummocky cross-stratifications), wave ripples	Rare bioclasts	Rare bioturbation	Storm deposits, Offshore/ Profundal
S10: Dark silty shales	Dark silty shales	Thinly laminated	N/A	Rare bioturbation	Offshore/Profundal
M1: Green shales	Green brown shales to very fine-grained sandstones	Tabular laminated beds, occasional wave and current ripples	N/A	Root traces, rare coal clasts, dessication cracks, strongly bioturbated	Mudflat/Palustrine

(Continues)

TABLE 1 (Continued)

Facies	Lithology/Texture	Sedimentary structures/Bedform	Skeletal components	Non-skeletal components	Environmental interpretation
M2: Silty ostracod wackestone	Silty bioclastic wackestone	Occasional current ripples	Abundant ostracods	Charophytes	Eulittoral/Foreshore
M3: Sandy gastropod floatstone	Sandy to silty floatstone	No structures	Abundant multimillimetre to centimetre preserved gastropods	N/A	Protected eulittoral
M4: Sandy gastropod/ooid grainstone to rudstone	Sandy grainstone to rudstone	Decimetre to multidecimetre-thick beds with wave ripples, sigmoidal cross-bedding, current ripples	Rare bioclasts	Ooids, charophytes	High energy eulittoral to supralittoral
M5: Sandy oolitic grainstone	Sandy oolitic grainstone	Multidecimetre to metre-thick beds with erosive base, flat top, sigmoidal cross-bedding with mud drapes, wave ripples on top	N/A	Coated quartz grains, ooids, intraclasts, quartz grains	High energy littoral
M6: Grey silty mudstone	Grey silty mudstones	Thinly laminated, rare current ripples, occasional slumps	Rare ostracods	Rare bioturbation	Offshore/Profundal
M7: Black shale to mudstone	Black organic-rich shales to mudstones	Thinly laminated	N/A	N/A	Offshore/Profundal
C1: Peloid/ Lithoclast packstone	Densely packed poorly sorted packstone	Erosive base decimetre-thick sheet-like beds; Rare wave ripples on top of beds	N/A	Rounded to sub-rounded peloids, sub-angular to sub-rounded lithoclasts, stromatolite chips, rare extraclasts	Eulittoral
C2: Gastropod/ Ooid grainstone to rudstone	Grainstone to rudstone	Sharp based multidecimetre-thick sheet-like beds with wave ripples on top	Gastropods	Ooids, intraclasts	Eulittoral to littoral
C3: Coated ostracod packstone to grainstone	Packstone to grainstone	Decimetre to multidecimetre beds with wave ripples and current ripples	Coated ostracods	Rare ooids and intraclasts	Eulittoral to littoral
C4:Grapestone/ Ooid packstone to grainstone	Packstone to grainstone	Multidecimetre beds with abundant wave ripples	N/A	Aggregates of ooids surrounded by oolitic cortex, rare stromatolite clasts	High energy eulittoral
C5: Oolitic grainstone	Grainstone	Sharp base decimetre to metre-thick beds with sigmoidal cross-bedding, wave ripples on the top	Disarticulated ostracods, bioclasts	Ooids, rare peloids, rare quartz grains	High energy eulittoral, shoal

(Continues)

TABLE 1 (Continued)

Facies	Lithology/Texture	Sedimentary structures/Bedform	Skeletal components	Non-skeletal components	Environmental interpretation
C6: Green silty dolomitic marls to mudstone	Silty dolomitic marls/mudstones	Massive multidecimetre to metre beds with occasional planar laminations and current ripples	N/A	Coal fragments, bioturbation, dessication cracks	Infralittoral
C7: Bioturbated mudstone to wackestone	Mudstone to packstone	Thinly laminated decimetre to metre-thick beds, occasional current ripples and wave ripples	Rare ostracods and gastropods	Bioturbation, rare quartz grains; dessication cracks	Low energy eulittoral to supralittoral (mudflat)
C8: Intraclastic breccia	Rudstone	Multicentimetre-thick lag	N/A	Mud clasts, stromatolite clasts, rare oncoids and oolites,	High energy littoral to supralittoral
C9: Oncoid rudstone	Rudstone	Multidecimetre to metre-thick discontinuous beds with sigmoidal cross-bedding and wave ripples on top	N/A	Stromatolite clasts, rare ooids and oolites, rare quartz grains; dessication cracks on top of beds	High energy littoral to supralittoral

across the basin. In this article, a correlation transect that illustrates the stratigraphic architecture of the Yacoraite Formation across the basin shows only three detailed interpreted sedimentological sections, but the transect is constrained with 27 sections which are not displayed for greater legibility. A set of 100 thin sections were analyzed to determine facies. All thin sections were stained with alizarin red-S to differentiate carbonate minerals (aragonite and calcite are stained, while dolomite remains unstained; Dickson, 1966) and with potassium ferricyanide to determine the distribution of ferrous iron.

Pre-microscopic observations were carried out under reflected and transmitted light with a binocular microscope (Nikon SMZ 800) to provide a large-scale view of the samples and characterize their general texture and porosity distribution. Petrographic observations followed using a Nikon Eclipse LV100 POL microscope.

The description of the carbonate allochthonous facies has been based on the Dunham (1962) classification scheme. The depositional texture and the different allochems are described in detail. Twenty-four lithofacies were defined by texture, sediment components, sedimentary structures, fossils and/or trace fossils (when present). These facies were grouped into 10 facies associations, defined and then attributed to a specific depositional environment on the basis of their elementary constituent facies, vertical stacking, lateral facies changes and overall geometry.

4 | RESULTS

4.1 | Facies analysis of the Yacoraite Formation

A synthetic depositional model based on facies descriptions (Table 1), facies associations (FA, Table 2) and interpretations in terms of depositional environments in a lacustrine setting is proposed.

The depositional model can be subdivided into two end-menders with a siliciclastic-dominated margin and a carbonate-dominated one. Mixing of both sources is possible, forming mixed facies. The siliciclastic-dominated facies are mainly located along previous footwall margins in the western part of the basin, whereas the carbonate-dominated ones preferentially occur in palaeohighs located away from siliciclastic input. Ten genetically related facies associations identified are detailed in Table 1.

4.1.1 | Clastic-dominated facies associations

FA1 Alluvial deposits

The alluvial deposits consist of fluvial and floodplain deposits. The fluvial deposits are made up of erosion-based, poorly

TABLE 2 Facies associations with facies stacking

FA	FA1 - Alluvial (Fluvial-Floodplain, S1, S2, S3)	FA2 - Deltaic (S4, S6)	FA3 - Sandflat (S5, S6, M4, M5)	FA4a - Shoreface (F8, F9)	FA4b - Low energy shore (S8, M4, M5)	FA5a - Offshore / FA5b - Profundal (S10, S9, M6, M7)
Facies	S1: Massive gravelly sandstones	S4: Medium to coarse-grained sandstones with large steep-angled tabular cross- stratifications, bioturbation	S5: Alternating silt and fine-grained sandstones, with wave and current ripples.	S7: Medium to coarse-grained sandstones with plane parallel to low-angle cross-bedding	S8: Fine to medium grained sandstones with plane parallel to wave ripples	S10: Siltstones, mudstones / Marls with rare HCS, slumps
	S2: Med. to Coarse gr. sandstones with trough Cross-bedding	S6: Medium to coarse-grained sandstones with sigmoidal cross-bedding (occasionally bidirectional)	S6: Medium to coarse-grained sandstones with sigmoidal cross-bedding (occasionally multi-directional)	S9: Fine to medium grained sandstones with HCS	M4: Sandy Gastropod / ooid grainstone to rudstone	S9: Fine to medium grained sandstones with HCS
	S3: Red siltstones with rootlets		M4: Sandy Gastropod / ooid grainstone to rudstone		M5: Sandy oolitic grainstone	M6: Grey-blue silty mudstone
			M5: Sandy oolitic grainstone			M7: Black organic-rich shales
Vertical distribution and stacking pattern	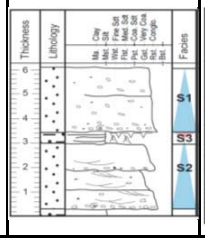	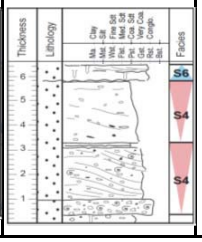	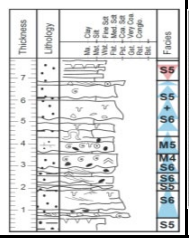	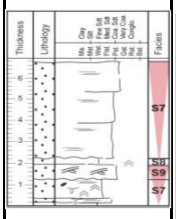	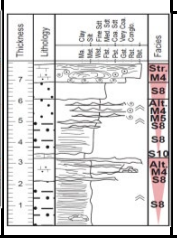	FA5a - Offshore 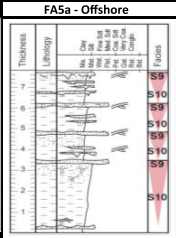 FA5b - Profundal 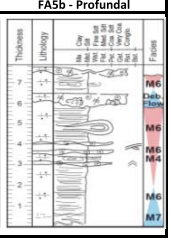

FA	FA6 - Mixed mudflat (C4, C7, M1, M4, M5, S6)	FA7 - High energy eulittoral (C5, C3, M4, M2)	FA8 - Low energy eulittoral (M2, C2, C5, C9)	FA9 - Oolitic bank (C5, C3, C9, M6)	FA10a - Alternating marginal (C1, M3, C6, C4, C8, C9)	FA10b - Alternating central (C8, M7, C6, C4)
	C4: Grapestone ooid grainstone to Packstone	C5: Oolitic grainstone	M2: Ostracod wackestone	C5: Oolitic grainstone	C1: Peloidal/lithoclast packstone	C8: Intraclastic oncoidal breccia
	C7: Laminated/bioturbated mudstone to wackestone	C3: Coated ostracods grainstone to packstone	C2: Gastropod Ooid grainstone to rudstone	C3: Coated ostracods grainstone to packstone	M3: Sandy to silty gastropod floatstone	M7: Black organic-rich shales to mudstone to wackestone
	M1: Green to brown shales	M4: Sandy Gastropod / ooid grainstone to rudstone	C5: Oolitic grainstone	C9: Oncoid rudstone	C4: Grapestone-ooids grainstone to packstone	C6: Green silty dolomitic marls to mudstone
	M5: Sandy oolitic grainstone	M2: Ostracod wackestone	C9: Oncoid rudstone	M6: Grey-blue silty mudstone	C6: Green silty dolomitic marls to mudstone	C4: Grapestone-ooids grainstone to packstone
	M4: Sandy gastropod / ooid grainstone to rudstone	C9: Oncoid rudstone			C8: Intraclastic oncoidal breccia	
	S6: Med. to coarse-grained sandstones with sigmoidal cross-bedding (occasionally bidirectional)				C9: Oncoid rudstone	
Vertical distribution and stacking pattern	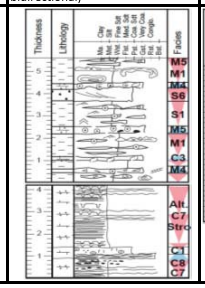	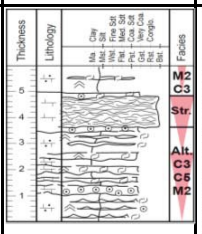	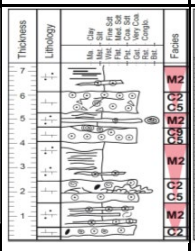	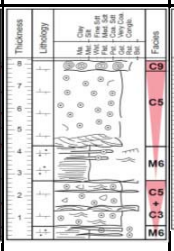	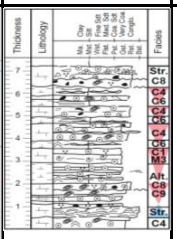	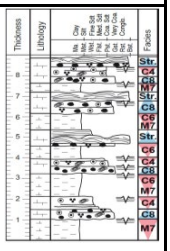

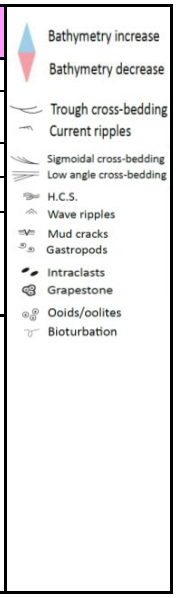

sorted, massive gravel beds (Facies S1, Figure 4A and Table 1), with medium to coarse-grained sandstones, organized in metre-thick fining-upward sequences, showing trough cross-stratifications, and current ripples at the top (Facies S2, Figure 4B and Table 1). A basal pebble lag is frequently observed as are channel-like geometries. These sandstones are embedded within reddish silty shales and rippled siltstones with root traces (Facies S3, Figure 4C and Table 1), delimited by the erosional surfaces present at the base of facies S1 and S2.

This Facies Association (FA) is interpreted as alluvial deposits, with fluvial channels and bars (S2 and S1, respectively) deposited within floodplain deposits (S3), and can be vertically stacked in sequences several metres thick, as shown in Table 2. The alluvial deposits are mostly located on the western margin of the Alemania-Metán sub-basin, where the western rift shoulder of the system supplies clastics eastwards into the basin.

FA2 Deltaic deposits

The delta front facies association is mainly composed of S4 facies (Tables 1 and 2) that corresponds to medium to coarse-grained sandstone with large steep-angled tabular stratifications (Figure 4D), organized in coarsening-upward sequences several metres thick, bioturbated on top and with abundant gastropods. The S4 facies (Table 1) are often associated laterally with medium to coarse-grained sandstones with mud-draped, multidirectional cross-stratifications (Facies S6, Table 1, Figure 4F), organized in metre-thick to several decimetres-thick coarsening-upward beds, reworked by wave ripples on their top (Figure 4F) and highly bioturbated.

Facies S4 is interpreted as delta front deposits prograding into a shallow lake system, supplied by fluvial systems upstream (Facies S2). Facies S6 is interpreted as longshore bars/sandbars in front of or laterally adjacent to the delta front systems, deposited by reworking both by

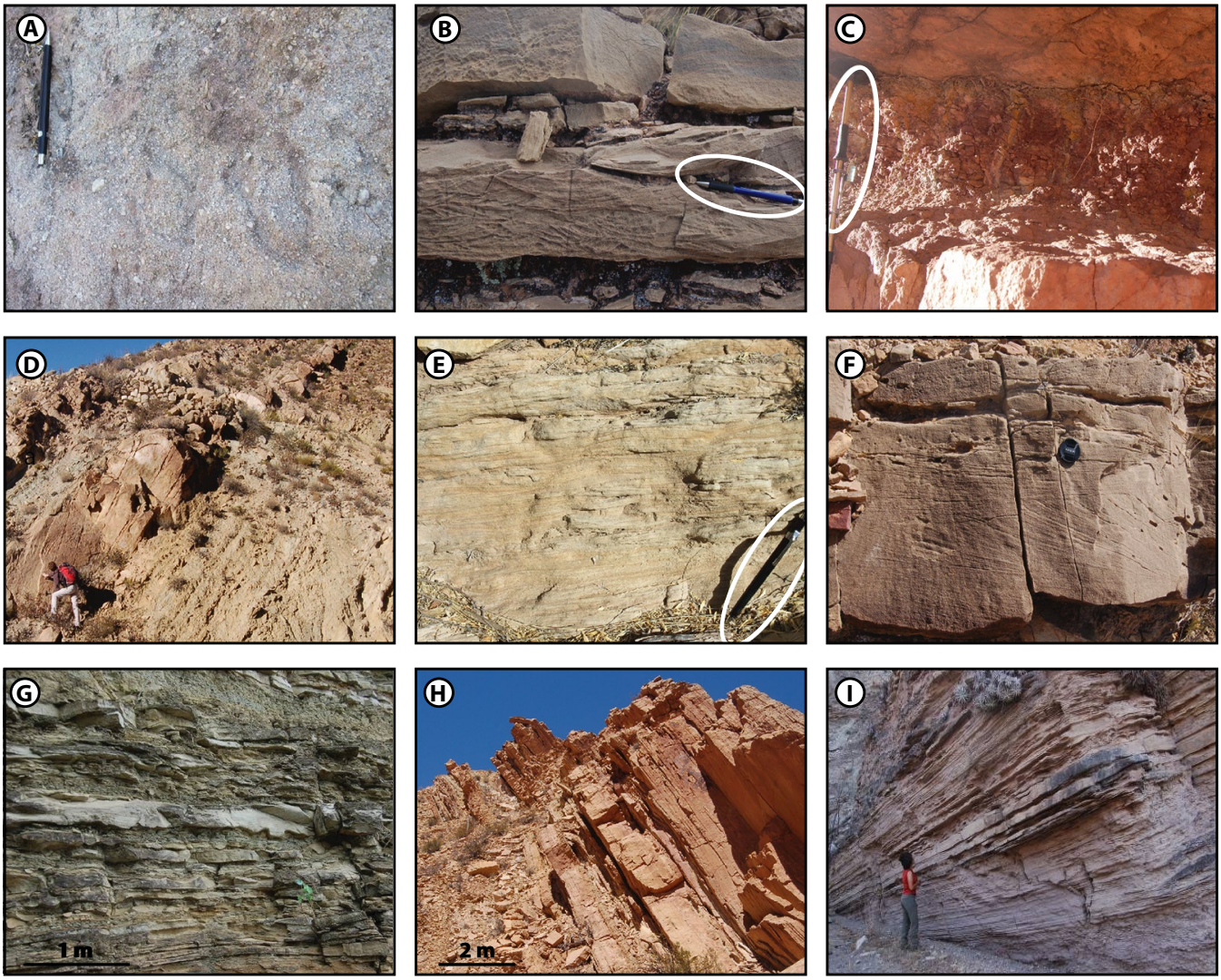

FIGURE 4 Siliciclastic facies illustrations, with: (A) massive gravelly to coarse-grained sandstone (facies S1); (B) medium to coarse-grained sandstone with trough cross-stratifications (facies S2); (C) red siltstones with root traces (facies S3); (D) coarse-grained sandstones with steep-angle tabular cross-bedding (facies S4); (E) silts and fine-grained sandstones with wave and current ripples (facies S5); (F) medium to coarse–grained sandstones with sigmoidal cross-stratification (facies S6); (G) medium to coarse-grained sandstone with plane parallel to low angle cross-stratifications (facies S7); (H) fine to medium-grained sandstones with horizontal bedding to wave ripples (facies S9); (I) fine to medium-grained sandstones with hummocky cross-stratifications (facies S9) interbedded with wave rippled silts (facies S10)

waves and probable longshore currents. They represent stacked sequences several metres thick, as shown in Table 2.

FA3 Sandflat deposits

This facies association is composed of alternating thinly laminated siltstones to fine-grained sandstones with both wave and current ripples (Figure 4E), showing numerous levels of desiccation cracks (Facies S5, Table 1). These facies are organized into 1 m to several metres-thick intervals, often cut by cross-bedded, bioturbated, medium grained sandstones (S6 facies). Facies S5 can also be associated with thin beds of gastropod-rich, sandy grainstones with wave ripples (Facies M4, Table 1, Figure 5F,G) to ooid-rich, sandy grainstones (Figure 5I), and centimetre-thick, wave-rippled beds of oolitic grainstones (Facies M5, Table 1, Figure 5H).

This facies association is interpreted as a sandflat deposited at the transition between the supralittoral and the eulittoral zone (highlighted by the presence of frequent exposure episodes underlined by the surface desiccation cracks), in a high-energy environment with significant clastic supply. Facies M4 and M5 are interpreted as storm lag deposits reworking carbonate-dominated deposits (Dukle, 1985; Chuanmao *et al.*, 1993), probably present in areas more distant from the clastic input. This sandflat facies association is also interpreted as being preserved laterally in the deltaic systems (Galloway, 1975; Dalrymple, 2010), in the clastic-dominated margin of the lake system.

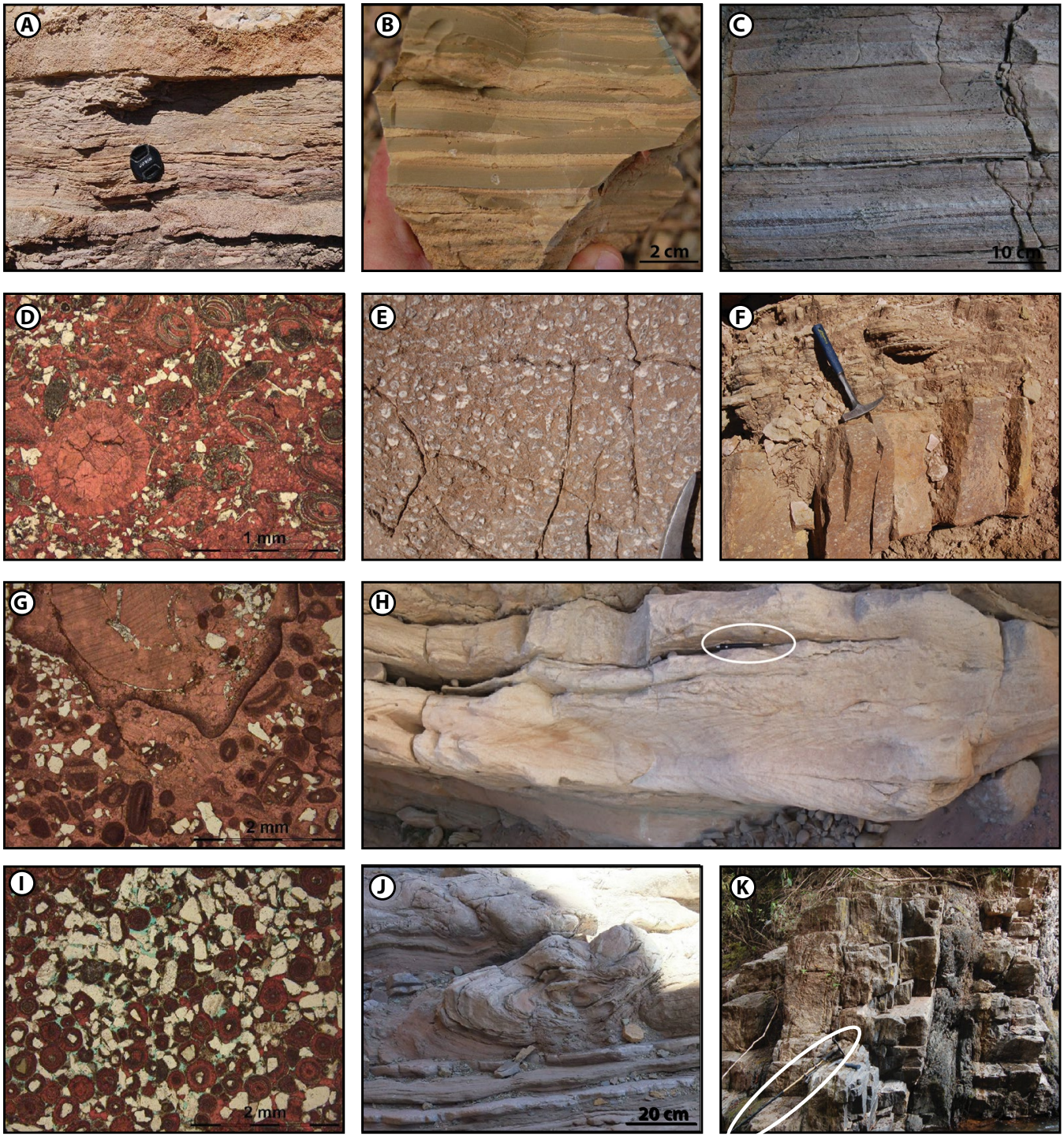

FIGURE 5 Mixed carbonate/siliciclastic facies illustrations, with: (A) green shales with rippled sandstones (facies M1); (B) green laminated shales alternating with rippled sandstone (facies M1); (C) silty ostracod wackestone (facies M2); (D) silty to sandy gastropod floatstone (facies M3); (E) sandy to silty gastropod floatstone (facies M3); (F) sandy gastropod-rich ooid grainstone to rudstone (facies M4); (G) sandy gastropod-rich ooid grainstone to rudstone (facies M4); (H) Sandy oolitic grainstone (facies M5); (I) sandy gastropod-rich ooid grainstone to rudstone (facies M4); (J) Grey blue overturned silty mudstone (facies M6); (K) black shales to mudstone (facies M7)

FA4 Shoreface deposits

This facies association can be subdivided into two end-members:

- FA4-a is characterized by the vertical stacking of fine to medium-grained sandstones with hummocky cross-stratifications at the bottom (Facies S9, Table 1, Figure 4G), passing transitionally to coarsening–upward, medium to coarse-grained sandstones (Figure 4H). This sequence can reach up to 7 m in thickness.

- FA4-b corresponds to the vertical stacking of fine to medium-grained sandstones several metres thick showing wave ripples to plane-parallel stratifications (Facies S8, Table 1, Figure 4H), alternating with decimetre-thick sandy oolitic grainstone lenses showing wave ripples on the top (Facies M5, Table 1, Figure 5H), passing transitionally upward to sandy gastropod/ooid grainstones to rudstones (Facies M4, Figure 5F, G and I) with occasional stromatolite beds (Table 1).

Facies Association 4-a is interpreted as a prograding shoreface (Table 2) in a high-energy environment dominated by waves with frequent storm events.

Facies Association 4-b can be interpreted as a low-energy shore/eulittoral environment, where local environmental conditions occasionally allowed the development of carbonate grains (oolites), fauna (gastropods) and stromatolites. Facies S8, M4 and M5 are frequently stacked to form prograding sequences several metres thick, as shown in Table 2.

FA5 Offshore/Profundal deposits

The Offshore/Profundal facies association can be divided into two subcategories:

- FA5a is dominated by thinly laminated, silty shales (Facies S10, Table 1), with occasional hummocky cross-stratifications (Facies S9), forming coarsening-upward cycles of dark silty shales over several metres. Hummocky cross-stratification increases vertically (Table 2).
- FA5b is dominantly made up of thinly laminated, gray silty mudstones (Facies M7, Table 1, Figure 5H), occasionally alternating with black organic-rich shales (Facies M6, Table 1, Figure 5G). They are organized into metre-thick coarsening-upward trends from black shales (Facies M7) passing upwards to gray silty mudstones (Facies M6) showing rare decimetre-thick slumped beds and creeping ball structures, occasionally capped by lenses of gastropod/ooid-rich grainstones with hummocky cross-stratifications (Facies M4).

Both FA5a and FA5b are interpreted to have formed in offshore or profundal lacustrine environments in a very low-energy domain, with rare storm events that deposited thin hummocky cross-stratification lenses (Zhang *et al*., 1998). Laminae preservation suggests an environment almost without bioturbation, and the organic-rich content preserved suggests restricted conditions, with low circulation that is locally disoxic, typical for a low-energy offshore domain in the profundal zone (Camoin *et al.*, 1997).

4.1.2 | Carbonate-dominated facies associations

The carbonate-dominated facies associations are dominantly located in the eastern part of the studied area, where the Guachipas palaeohighs are located (Figure 2), allowing carbonate sedimentation to ocur far away from the siliciclastic sources.

FA6 Mixed mudflat deposits

In the siliciclastic-dominated margin of the basin to the west, the mudflat depositional environment is dominated by green to brown shales (Facies M1, Table 1, Figure 5A,B), forming decimetre to metre-thick tabular beds. These green shale facies are highly bioturbated, and show abundant desiccation cracks. The M1 facies often contain coal fragments, and are generally associated with centimetre-thick lenses of sandy, oolitic grainstone beds with wave and current ripples (Facies M5, Table 1, Figure 5H, I). Decimetre-thick, medium to coarse-grained sandstone beds with sigmoidal megaripples (Facies S6, Table 1) are occasionally observed in the clastic-dominated margin of the basin.

In the carbonate-dominated part of the basin (Figure 2), the mudflat facies association is mainly composed of bioturbated mudstone to wackestone (Facies C7, Table 1) associated with lenses of grapestone/ooid packstones with wave ripples (Facies C4, Table 1; Figure 6F,G). The abundant desiccation cracks are generally associated with intraclastic breccia made up of stromatolite fragments (Facies C8, Table 1; Figure 6K), and intercalated thinly laminated stromatolites.

The predominance of pelitic facies (Facies M1 and C7) indicates a dominant process of decantation of mud under very shallow water depth, with the development of microbial film resulting in the formation of thin and thinly laminated stromatolites. Frequent desiccation cracks suggest periodic exposure, forming dry mudflats (Hardie *et al.*, 1978). The bad preservation of laminae correlates with the abundance of bioturbation. The intercalation of grainy material (oolitic, sandy grainstones and grapestones to ooid grainstones) with wave ripples, and stromatolite clast breccia, indicates reworking of ex-situ material by occasional strong waves during storm events.

FA7 High-energy eulittoral/carbonate shoreface deposits

This facies association is characterized by the dominant occurrence of a well-sorted grainy facies, e.g. wave-rippled oolitic grainstones (Facies C5, Table 1), coated-ostracod grainstones to packstones (Facies C3, Table 1, Figure 6D,E), and sandy gastropods and ooid grainstones to rudstones with wave ripples (Facies M4, Table 1). The facies stacking is organized in coarsening-upward successions several metres thick, starting with ostracod wackestones (Facies M2, Table 1, Figure 5B,C) at the base, passing upwards to grainy facies (Facies C5 and C3). These cycles are occasionally topped by stromatolites several decimetres thick (Table 2).

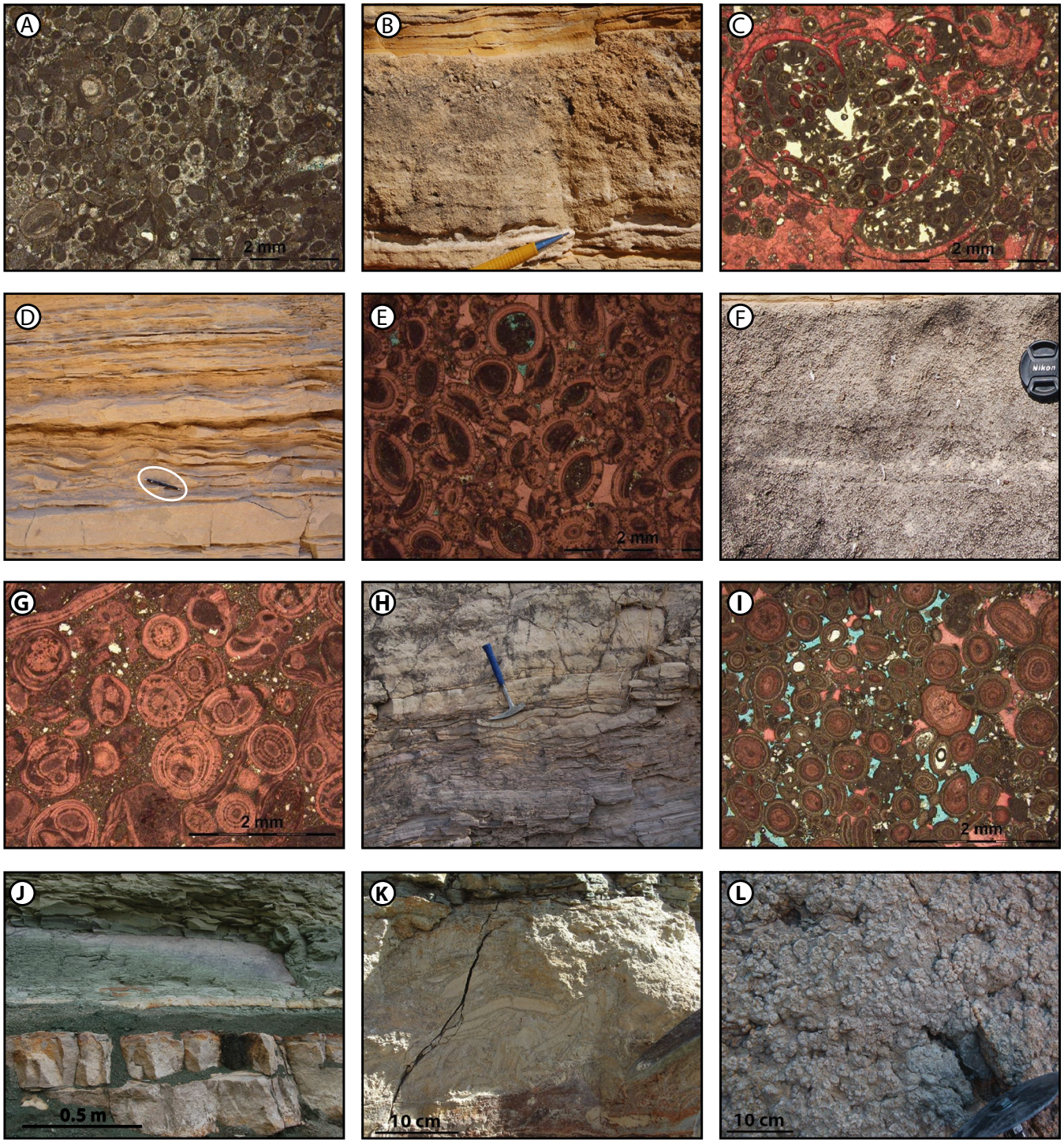

FIGURE 6 Carbonate dominated facies illustrations, with: (A) photomicrograph showing peloid to lithoclast packestone (facies C1); (B) field photograph of gastropod-ooid grainstone to rudstone (facies C2); (C) photomicrograph showing gastropod-ooid grainstone to rudstone (facies C2); (D) field photograph of coated ostracod grainstone to packestone (facies C3); (E) photomicrograph showing coated ostracod grainstone to packestone (facies C3); (F) field photograph of grapestone-ooid grainstone to packestone (facies C4); (G) photomicrograph showing grapestone-ooid grainstone to packestone (facies C4); (H) field photograph of oolitic grainstone (facies C5); (I) photomicrograph showing oolitic grainstone (facies C5); (J) Silty dolomitic marls to mudstones; (K) field picture of intraclastic oncoidal breccia (facies C8); (L) field picture of oncoid rudstone (facies C9)

Grainy textures (well-sorted and grain-supported) and sedimentary structures (wave ripples) indicate a high-energy environment influenced by wave energy, compatible with shore environments in the eulittoral zone (Arp, 1995; Clausing, 1990). This FA7 is organized into prograding trends several metres thick in a carbonate shore environment (Table 2).

FA8 Low-energy eulittoral deposits

This facies association is dominantly composed of ostracod-rich, silty wackestones with charophytes and occasional wave ripples (Facies M2), with occurrences of decimetre-thick gastropod and ooid–rich wave-rippled grainstone beds (Facies C2, Table 1, Figure 6B,C; and C5 Facies), showing occasional oncoid rudstone on top (Facies C9, Table 1, Figure 6L). The stacking of this facies corresponds to metre–thick prograding sets of silty mudstones (M2) passing upwards to grainy carbonates (Facies C3 and C5), as shown in Table 2.

This facies association is interpreted as a low-energy eulittoral setting. The significant detrital fraction in the finest sediments suggests clastic sources in the near vicinity. The presence of ostracods and charophytes is also associated with lake shore environments (Flügel, 2004). The occurrence of rippled grainstones on top of laminated silty mudstones can be interpreted as being deposited during periods of more intense wave energy, preventing fine particles from being deposited.

FA9 Oolitic bank deposits

Facies association 9 mainly corresponds to the deposition of thick (several metres thick) sheet-like beds of oolitic grainstones (Facies C5, Table 1), with a sharp base, large-scale sigmoidal megaripples and wave ripples on top of the beds. The facies are associated with coated-ostracod grainstones (Facies C3) and occasionally with oncoid rudstones (Facies C9) on top of the beds (Table 2). The lateral extent of these beds is on the order of kilometres with the facies association organized into lenses forming positive sedimentary geobodies. They can be stacked together forming metre-thick packages.

Textures (well-sorted, grain-supported) and sedimentary structures (cross-bedding, wave ripples) indicate a high-energy environment, characterized by strong currents and wave energy. The absence of desiccation features also indicates permanent subaqueous conditions. Williamson and Picard (1974) described such facies in the Green River Formation and interpreted it as shoal or oolitic bank deposits, prograding in a littoral environment.

FA10 Highly alternating deposits

Within the Yacoraite Formation, highly alternating patterns in the sediment stacking could be identified either in the basin centre or along the margins on both siliciclastic and carbonate-dominated margins:

FA10a Highly alternating marginal lacustrine. The highly alternating marginal facies association is characterized by the sharp superposition of coarse-grained grainstone to packstone facies (Facies C1, Table 1, Figure 6A; Facies C4), and silty dolomitic marls to mudstones (Facies C6, Table 1, Figure 6J; Table 2). Occasional intraclastic breccia (Facies C8, Table 1, Figure 6K), gastropod-rich floatstones (Facies M3, Table 1, Figure 4E), and oncoid rudstones (Facies C9, Table 1, Figure 6L) are present as lags at the base and on top of the grainstone to packstone beds, associated with desiccation cracks. Thick stromatolites (up to 1 m thick) are also common on top of the grainstone/packstone beds.

The high-energy grainstone to packstone facies are thought to be deposited in the proximal part of the basin (e.g. eulittoral and littoral facies associations), whereas the silty marls to mudstones are interpreted as low-energy infralittoral deposits. The rudstones and breccia lags are thus recording the subaerial erosion or wave ravinement during, respectively, the lake-level drop and subsequent flooding.

FA10b Highly alternating central lacustrine. The highly alternating central lacustrine facies association is dominated by silty dolomitic marls to mudstones (Facies C6) and black organic-rich laminated shales to mudstones (Facies M7, Table 1, Figure 5H), with frequent, several decimetre-thick intercalations of grapestones and oolites with wave ripples, showing desiccation cracks at their base, that propagate into the C6/M7 facies below. Stromatolites, which may reach several decimetres in thickness, are also common on top of the grainstone beds (Table 2).

Dolomitic marls to mudstones (C6) and black organic-rich shales to mudstones (M7) are interpreted as infralittoral and profundal deposits, respectively (Camoin *et al.*, 1997), deposited by decantation processes in a very low-energy environment in the center of the basin. The grapestones and oolitic grainstones are deposited in a high-energy, wave-dominated environment, and the presence of desiccation cracks at their base suggest periods of exposure. Evidence of exposure in the center of the basin highlights the very significant fluctuations of the lake level.

4.2 | General depositional model of the Yacoraite Formation

Based on the vertical stacking pattern of facies associations and the stratigraphic architectures proposed from the correlation between measured sections, it is clear that the large-scale lacustrine system (*ca* 200 × 200 km in the Alemania-Metán sub-basin) occupying the Salta rift basin exhibited different depositional profiles depending on the location in the basin. The different depositional profiles that have been reconstructed from the facies analysis are summarized in Figure 7.

The predominance of shallow marginal facies (no extensive development of deep basinal facies) suggests a low to medium gradient ramp-type margin, rather than a bench-type margin (Platt and Wright, 1991). However, the proximity of the clastic input, the structural pattern, the proximity of the

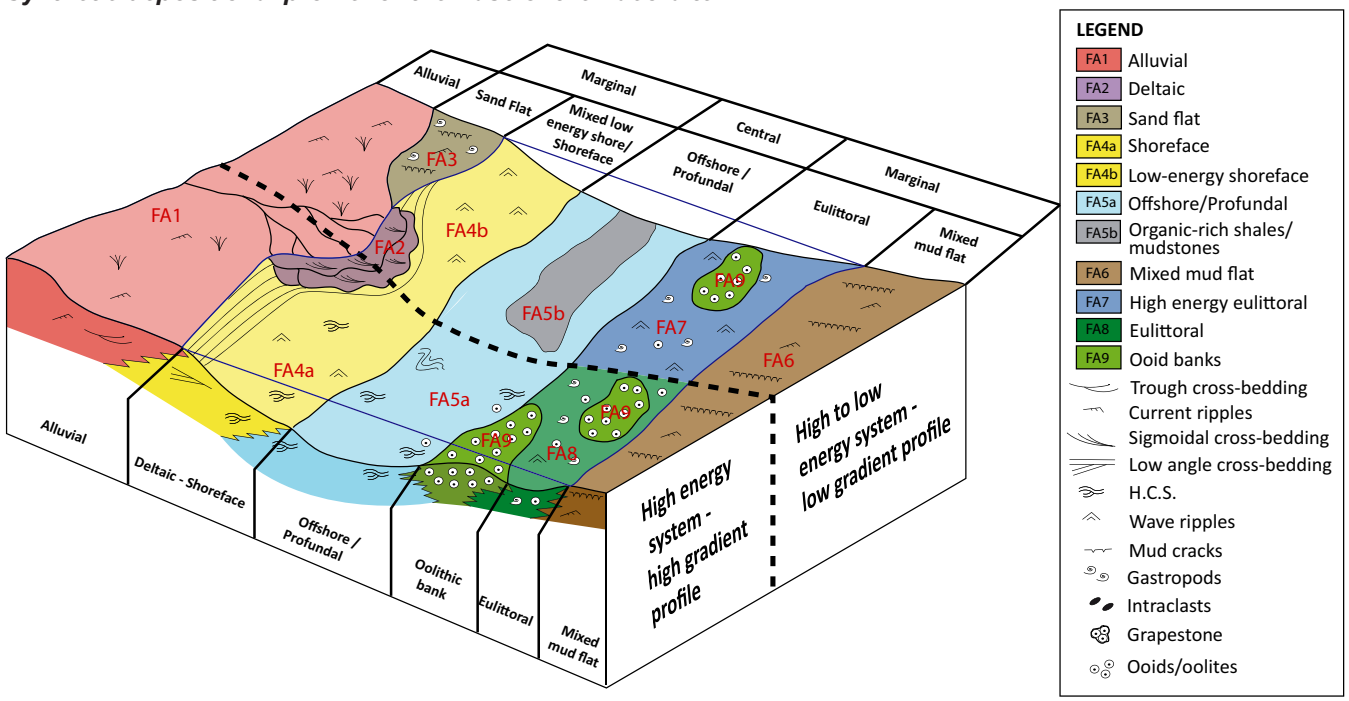

FIGURE 7 Synthetic composite depositional profile of the Yacoraite Formation, showing the relationships between the different end members (carbonate or clastic dominated environments) in high and low energy systems

potential connection with other lakes to the north, as well as the wave patterns had an impact on the facies association distribution and on the morphology of the depositional profiles.

4.2.1 | Siliciclastic-dominated areas

Siliciclastic, fluvial-dominated high-energy margin

The western part of the Salta Basin (Tintin, Cachi areas, Figure 2) is characterized by high-energy, siliciclastic-dominated environments. In the vicinity of river mouths, fluvial deposits (FA1) pass downstream to small deltaic lobes (FA2). Laterally, this siliciclastic material is reworked by wave action and forms sandflats (FA3) and low-energy shore deposits (FA4b). The deeper part of the profile is characterized by the siliciclastic-dominated offshore facies association (FA5; Figure 7).

Siliciclastic, low-energy margin

The southern part of the Salta Basin is characterized by low-energy, siliciclastic-dominated to mixed clastic and carbonate facies. Supralittoral to eulittoral sandflat (FA3) is the most proximal (shallow) environment (Figure 7). It passes downstream to siliciclastic shore deposits (low -energy – FA4b), characterized by a siliciclastic groundmass and a few carbonate occurrences. The deeper part of the profile is characterized by the siliciclastic-dominated to mixed clastic and carbonate-dominated offshore facies association (FA5).

4.2.2 | Carbonate-dominated areas

Carbonate, high-energy, low-gradient margin

The eastern part of the Alemania-Metán sub-basin (Cabra Corral area, Figure 2) corresponds to a structural high, at the time of deposition, located in the center of the Salta Basin. It is characterized by carbonate-dominated sedimentation and high-energy facies. The widespread occurrence of cross-bedded oolitic and bioclastic grainstones (FA9) constitute a local barrier that separate silty, ostracod-rich facies (low-energy eulittoral FA8) and mixed offshore facies (FA5), suggesting a locally 'barred' shoreline by discontinuous oolitic banks, such as that proposed by Eardley (1966) and Gwynn and Murphy (1980) for the modern Great Salt Lake. The most proximal and shallow environments are dominated by mixed mudflats (FA6) and low-energy eulittoral deposits (FA8) (Figure 7).

Carbonate, low-energy, low-gradient margin

This depositional profile is transitional between the carbonate-dominated, low-gradient, high-energy margin and the siliciclastic-dominated, low-gradient, low energy margin. It is observed in the southern part of the Alemania-Metán sub-basin (Cabra Corral South, Amblayo, Figure 2), but also along the shore of the Salta-Jujuy high (Figure 2). Ranked by increasing water depths, the facies associations observed along this profile are mixed clastic and carbonate-dominated mudflat (FA6), high-energy eulittoral carbonate facies (FA7

- grainy facies, ostracods, abundant stromatolites) and mixed offshore deposits (FA5).

4.2.3 | Highly alternating depositional system

The upper part of the Yacoraite Formation (Alemania Member) is characterized by a drastic change in the sedimentation pattern as well as the dynamic of the sedimentary system into a highly alternating system, which requires the definition of an additional specific depositional profile for the upper part of the Yacoraite Formation.

The highly alternating depositional system is defined by two facies associations, a highly alternating marginal facies (FA10a) and a highly alternating central facies (FA10b), based on the stacking of facies and facies associations that have been defined for the Alemania Member of the Yacoraite Formation in the eastern margin of the basin, as shown in Table 2. The inferred synthetic depositional profile is characterized by a mixed mudflat depositional environment (FA6) with occasional gastropod-rich ponds passing upward to a marginal lacustrine environment composed of low to high-energy eulittoral facies associations (FA7) with occasional oolitic banks (FA9). The marginal lacustrine domain passes distally to the central lacustrine domain, which is made up of silty marls deposited in an offshore environment (FA5a), with occasional oolitic and gastropod-rich grainstone to packstone banks (mixed between FA7 and FA9) intercalated. The main difference is the presence of black organic-rich silty shales in the very distal part of the central lacustrine domain, which may correspond to a potential source rock for the system, indicated by numerous desiccation cracks suggesting exposure and recurrent complete desiccation of the lake.

The western part of the profile is dominated by clastic deltaic deposits with fluvial mouth bars (FA1/FA2) and shoreface deposits (FA4a) passing distally to offshore (FA5a) environments, similar to the depositional profile shown in Figure 7. The slope of this profile is assumed to be gentler than that of the lower part of the Yacoraite Formation, and the mean bathymetry is consequently reduced in the upper part of the Yacoraite compared to the base.

The highly alternating pattern is defined in the eastern margin and in the central part of the basin where the rapid alternation of the proximal and distal facies and facies associations (Figure 8) are well-preserved. In the western clastic margin this rapid alternation is poorly observed due to the high-energy clastic system dominated by fluvial and wave erosion.

The highly alternating system is characterized by the basinward shift of these facies belts, which results in the sharp interbedding of facies associations from the proximal domain (mixed mudflat and marginal lacustrine) with distal facies associations from the central lacustrine domain, as shown in Table 2. This rapid alternation of proximal and distal facies is interpreted as being the result of rapid variations in lake level that induced a drastic downward shift of proximal facies (gastropod floatstone, peloid packstone, coated ostracod packstone to grainstone and stromatolites) onto the basinal domain, forming 'lowstand'-like wedges prograding towards the center of the basin (Figure 9A–D). Desiccation cracks are observed in the center of the basin, and this suggests complete desiccation of the system, with evaporation of the lake. During the subsequent lake-level rise, an intraclastic breccia was deposited as a lag draping the former deposits (Figure 9E), capped by offshore/profundal and marginal sedimentation deposited during high lake levels (Figure 9F).

It is assumed that these rapid lake-level variations with recurrent desiccation of the system are favoured because the mean bathymetry in the lake is reduced compared to the basal part of the Yacoraite Formation (e.g. Amblayo Member).

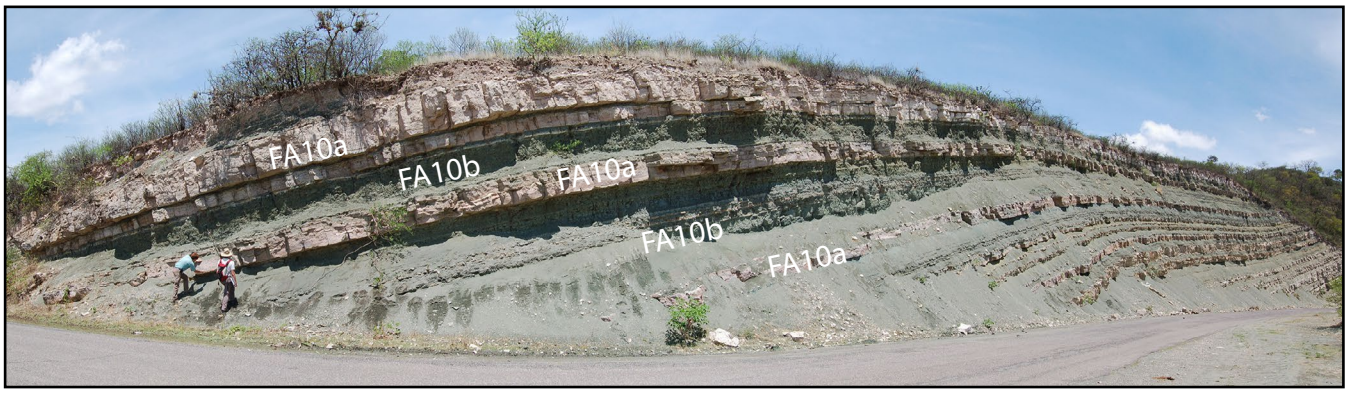

FIGURE 8 Outcrop picture showing alternation of FA10a and F10b in the topmost part of the Yacoraite Formation (Sequence 4, Cabral Coral section), illustrating the alternating depositional system

5 | STRATIGRAPHIC ARCHITECTURE OF THE YACORAITE

5.1 | Key surfaces

Key surfaces have been identified based on their diagnostic features, geometries and the facies association distribution. Sequence boundaries (SB) are characterized by an erosional base and often exposure in the proximal settings, a sharp basinward shift of the depositional system, and a sharp facies change from deep to very shallow facies in the basin axis. They can be superimposed onto the transgressive surface (TS) and ravinement surface (RS) along the basin margin. Maximum flooding surfaces (MFS) are characterized by maximum transgression of the depositional system, deepest facies in the basin axis and on the basin margin. They can be superimposed onto the transgressive surface and ravinement surface in the basin axis. Transgressive and ravinement surfaces (TS/RS) are characterized by a sharp and possibly erosional geometry and a rapid landward shift of the depositional system. They commonly correspond to multiple events, at the transition from the basin axis to the proximal settings.

The Yacoraite Formation recorded an overall transgressive trend, followed by a prograding, filling up trend (Cabra Corral reference section, Figure 10). The Yacoraite Formation can be subdivided into four main 'mid-term' sequences, each about 1 Myr duration (Figure 10), bounded by remarkable key surfaces.

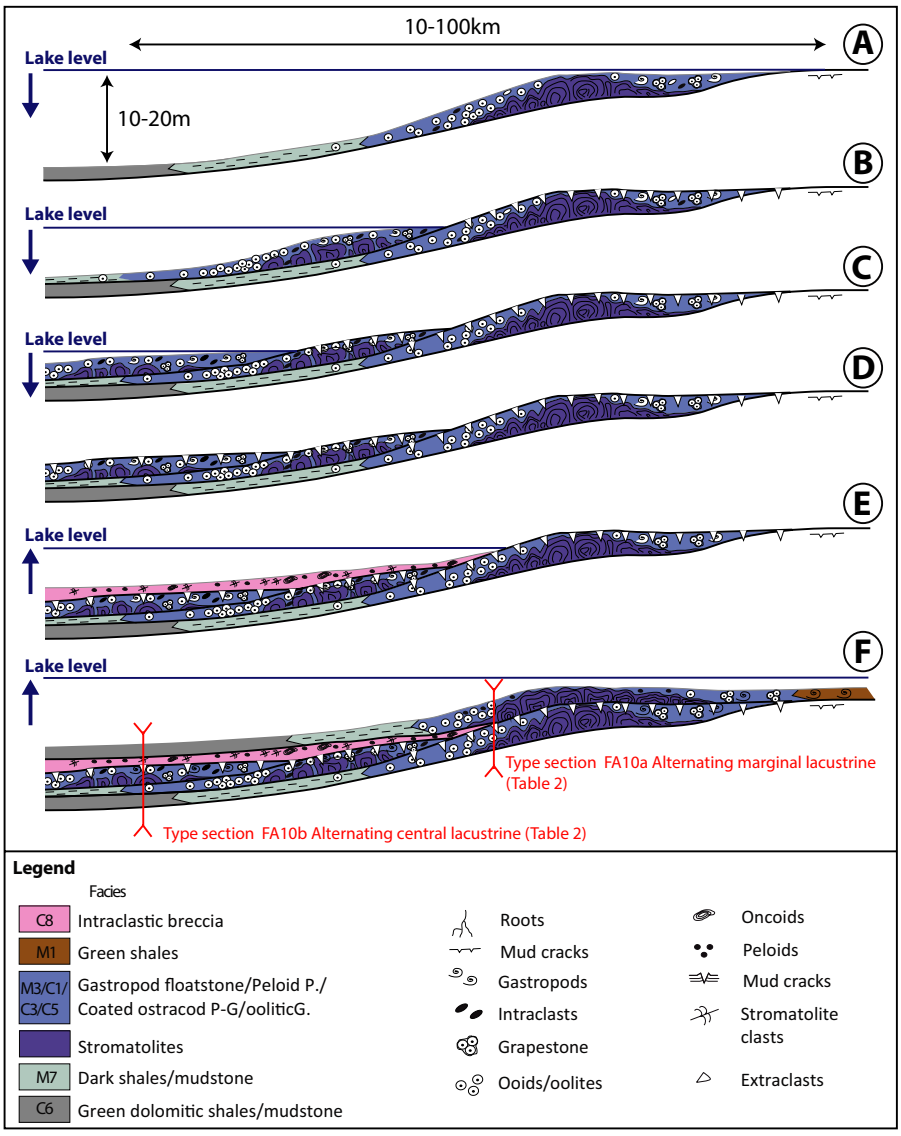

FIGURE 9 Eastern margin evolution of the topmost Yacoraite Formation (sequence 3b to sequence 4b, Alemania Member) in response to rapid lake-level variation

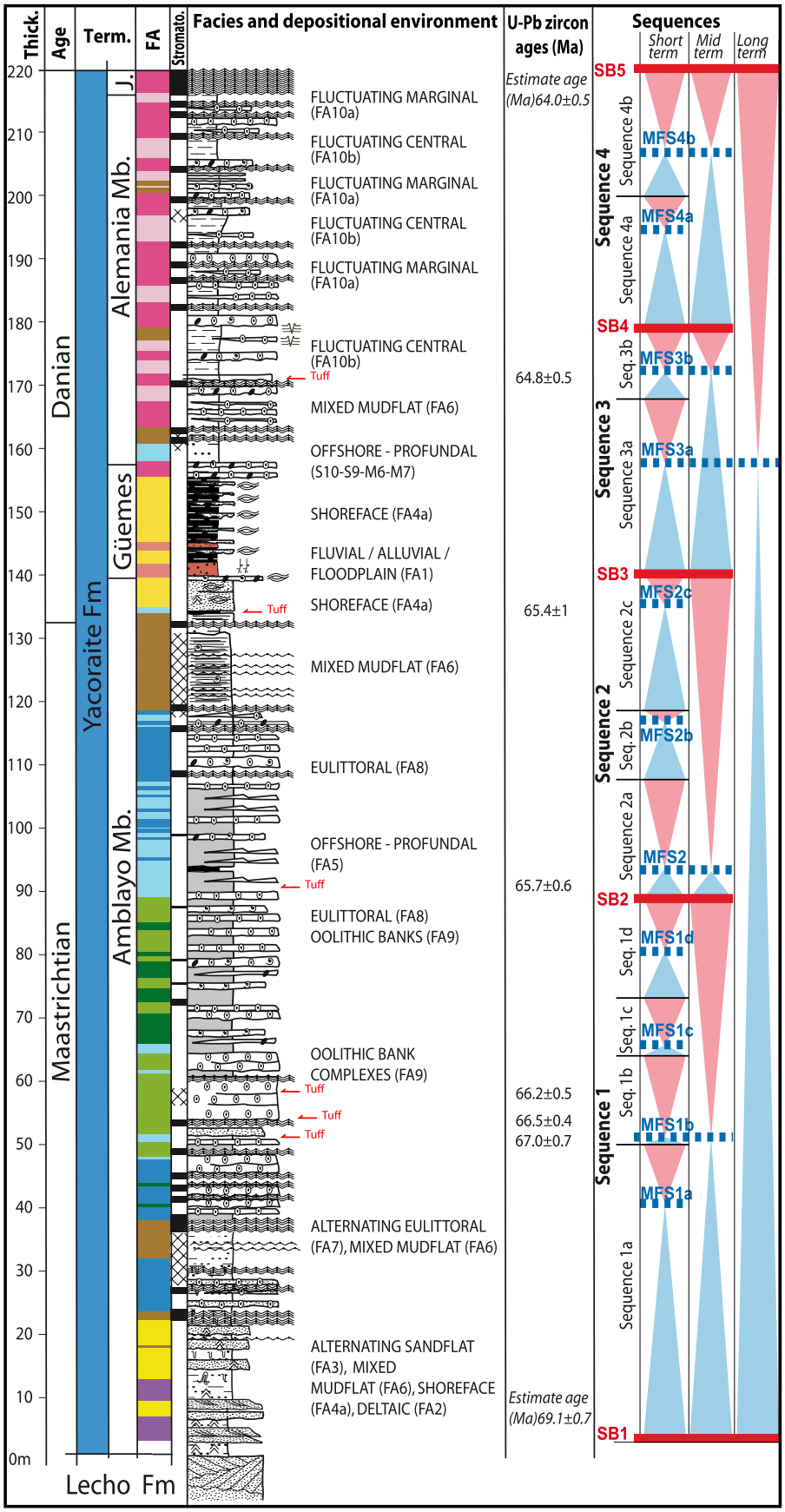

FIGURE 10 Reference sedimentological section of the Yacoraite Formation (Cabra Corral area) and correlation between lithostratigraphic members and sequence stratigraphy. The U/Pb zircon ages are projected according to the basin scale correlations

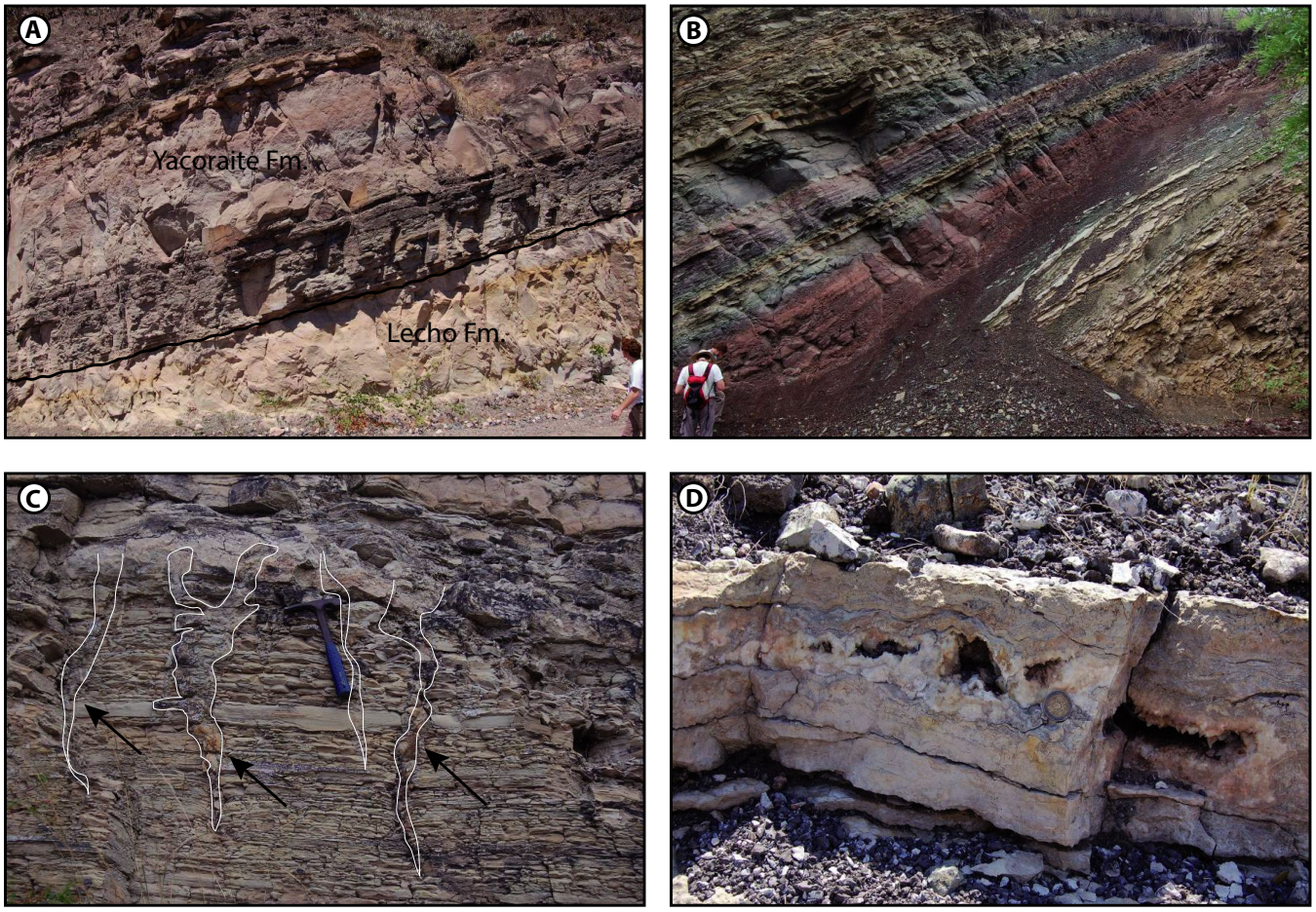

FIGURE 11 Field pictures of the main stratigraphic surfaces (sequence boundaries) observed in the field, with (A) SB1 separating the Lecho Formation and the Yacoraite Formation, (B) SB3 characterized by a basinward shift surface between clastic shore deposits and alluvial red beds, (C) SB4 corresponding to a major exposure surface marked by desiccation cracks, (D) SB5 marking the top of the Yacoraite Formation, marked by evidence of exposure with vugs and evaporate pseudomorphs

5.2 | Sequence definition and architecture

5.2.1 | Sequence 1

Sequence 1 is bounded at its base by a major sequence boundary (SB1), that corresponds to a combined sequence boundary with a transgressive surface (SB/TS1) onto the Lecho Formation (Figure 10). It is characterized by an erosional surface underlain by a thin lag onto the aeolian/fluvio-lacustrine deposits of the Lecho Formation (Figure 11A).

Sequence 1 is defined between SB1/TS1 and SB2 with maximum flooding (MFS1) recorded by widespread offshore deposits (Figure 10). A volcanic tuff/ash layer interbedded close to the MFS1b indicates an age of 66.2 ± 0.5 Ma to 66.5 ± 0.4 Ma (U/Pb zircon dating, Rohais *et al.*, 2019) in the Cabra Corral section. Sequence 1 has been subdivided into four higher order 'short-term' sequences, from Sequence 1a to 1d. These sequences are organized into an overall retrograding trend from mixed mudflat (FA6), to high-energy eulittoral (FA7) and oolitic bank complex (FA9) depositional systems. Each short-term sequence (1a to 1d) is organized into a prograding trend.

At basin scale, the base of Sequence 1 is organized into a long transgressive trend, which consists of mixed depositional environments dominated by deltaic, sandflat and mudflat facies associations (respectively FA2, FA3 and FA6). The transgressive trend of Sequence 1 is preserved in the central part of the basin and progressively onlapped by the basin margin and palaeohigh (Figure 12). Along the south-western margin, the depositional system is mainly characterized by fluvial and deltaic facies associations (FA1 and FA2). The maximum backstep of the deposits onto the basin margins and palaeohigh was reached during the deposition of Sequence 1d (Figure 12). This period corresponds to the maximum lateral and vertical extension of the oolitic bank complexes (Sequences 1C and 1D, Figure 12).

The Sequence 1 upper limit corresponds to sequence boundary 2 (SB2), characterized in the center of the basin (Cabra Corral area) by a sharp facies association change

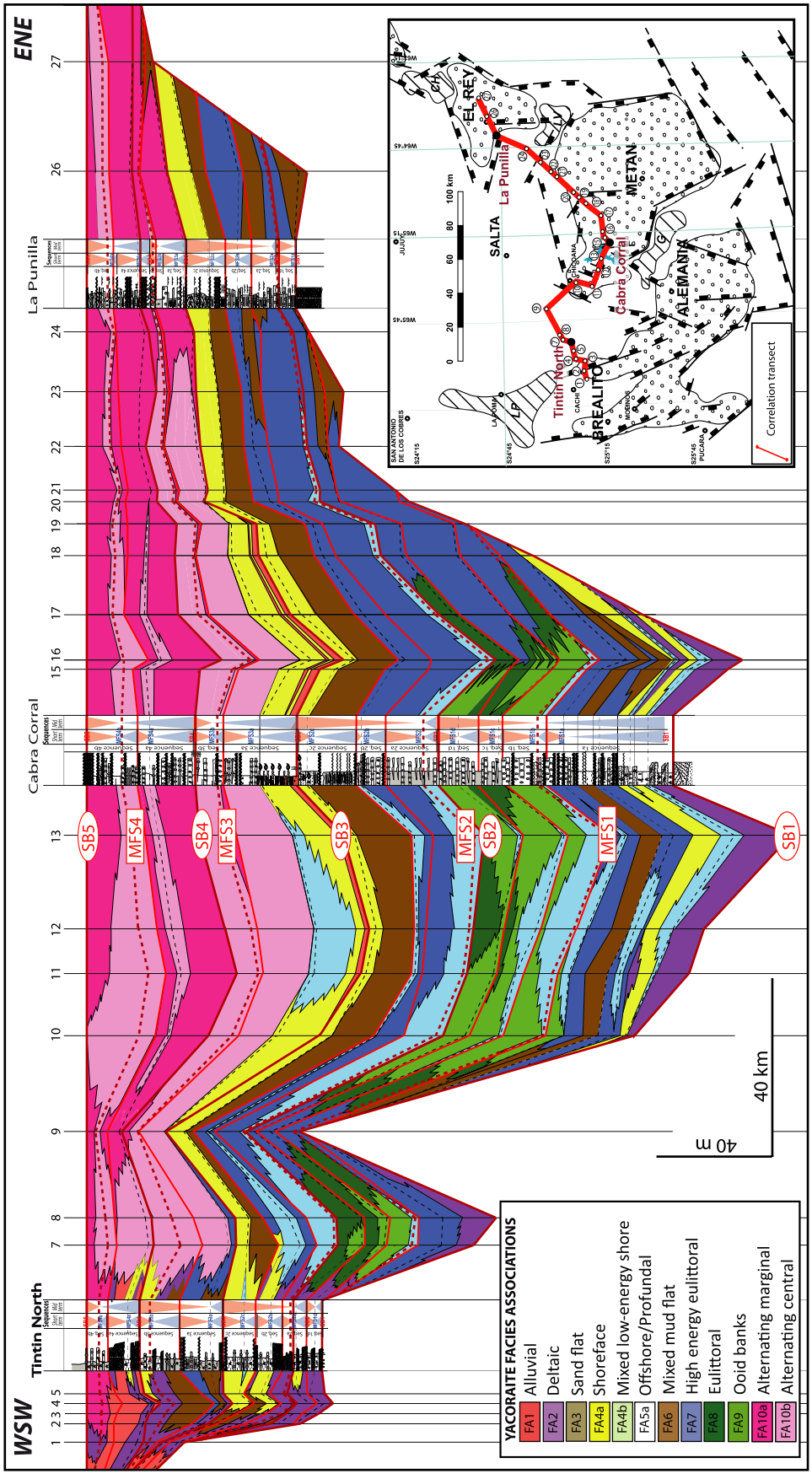

FIGURE 12 Correlation transect of the Yacoraite Formation across Alemania-Metan sub-basins

from oolitic bank deposits (FA9) and low-energy eulittoral deposits (FA8) to deeper facies (FA5). Therefore, this sequence boundary also corresponds to a transgressive surface.

5.2.2 | Sequence 2

Sequence 2 is defined between SB2 and SB3 with a maximum flooding (MFS2a) recorded by a thick interval (1–10 m thick) of offshore deposits (FA5). Sequence 2 is a mainly carbonate-dominated and extended distal facies recorded within the basal part of the Yacoraite Formation (Sequences 1–2). It is divided into three 'short-term' sequences, from Sequence 2a to 2c.

The base of Sequence 2 corresponds to a rapid retrogradation from eulittoral (FA8) to offshore facies (FA5) up to the main maximum flooding surface of Sequence 2 (MFS 2a). Above, no more oolitic bank complexes were deposited within Sequence 2, and the top of this sequence is characterized by progradational sets of mixed mudflat deposits (FA6) onto eulittoral deposits (FA8) reaching the center of the basin (Sequences 2a and 2b; Figure 12).

The top of the sequence is capped by an extended basin-wide blanket of shallow, wave-dominated, clastic eulittoral deposits below SB3 (FA4).

The top of Sequence 2 is marked by a drastic change in terms of sedimentation, with the deposition of clastic material, just below sequence boundary 3 (SB3) that marks the top of the sequence.

Sequence boundary 3 is characterized in the Cabra Corral area by a major facies association change from shoreface (FA4a) to fluvial/alluvial/floodplain (FA1), which documents a major basinward shift of the facies association marked by red palaeosoils (Figure 11B).

5.2.3 | Sequence 3

Sequence 3 is defined between SB3 and SB4 with a maximum flooding (MFS3 = MFS3b) that corresponds to the maximum flooding surface of the long-term cycle. The lower part of Sequence 3 is siliciclastic-dominated, while the upper part is carbonate-dominated. It recorded a major change in the depositional system, already announced by the shallow clastic shoreface deposited on top of Sequence 2, with evidence of lake desiccation in the central part of the basin (Cabra Corral area). Two short-term sequences were identified within Sequence 3, namely Sequences 3a and 3b.

A first transgressive trend is recorded by a transgressive siliciclastic shore (FA4—equivalent to the Güemes Member; Figure 12). The western and southern margin are characterized by an increase in the sediment supply with large aggrading deltaic packages (FA2). Then, following the first major flooding of Sequence 3a characterized by the highest total organic carbon (TOC) content within the Yacoraite Formation (Rohais *et al.*, 2019), the sedimentary dynamic drastically changed toward the highly alternating dynamic, with high frequency alternation of the proximal and distal facies with evidence of abundant desiccation cracks, mostly in the eastern and central part of the basin. The topmost part of Sequence 3 is characterized by a thick prograding deltaic package (FA2) with mudflats (FA6) and a low-energy shoreface (FA4b) laterally. The topmost part of Sequence 3 is also characterized by a thick prograding deltaic package (FA2) along the western margin, and alternating marginal facies associations (FA10a) in the eastern margin of the basin (far from the clastic sources), passing basinwards toward alternating central facies associations (FA10b; Figure 12).

The upper limit of Sequence 3 corresponds to sequence boundary 4 (SB4). In the Cabra Corral area, this surface is characterized by a major facies association change from mixed mudflat deposits (FA6), to highly alternating marginal deposits (FA10b) that document a major basinward shift. Large, metre-scale mud cracks occurring in the central part of the basin (Cabra Corral area) indicate a complete desiccation of the basin (see photograph in Figure 11C).

5.2.4 | Sequence 4

Sequence 4 is defined between SB4 and SB5 with a maximum flooding (MFS4b) characterized by a maximum transgression of the system during Sequence 4 (Figure 10). The lower part of Sequence 4 is carbonate-dominated, and recorded highly alternating lake levels with multiple layers of organic-rich deposits (FA5b).

Sequence 4 is divided into two sequences of aggrading to transgressive highly alternating trends (Sequences 4a and 4b), above which prograding highly alternating marginal onto highly alternating central facies associations fill the basin. This continues up to SB5, at which point alluvial and evaporite sedimentation begins in the basin marking the start of the Tunal Formation.

Sequence boundary 5 is characterized by a major basinward shift in the Cabra Corral area recorded by a major facies association change from highly alternating marginal (FA10a) to playa deposits (Tunal/ Olmedo Formations, Figure 3). Evidence of vugs and halite pseudomorphs (Figure 11D) in the basin axis indicate a drastic change in terms of sedimentation, from the lacustrine deposits of the Yacoraite Formation to the alluvial and evaporite deposits of the Tunal Formation.

6 | DISCUSSION

6.1 | Palaeogeographic evolution of the Yacoraite Formation in the Alemania—Metán sub-basins

Identified surfaces and sequences have been correlated at basin scale as shown in Figure 12. These correlations were used to establish a set of 12 *ca* 200 × 200 km palaeogeographic maps (Figure 13) for the Alemania-Metán sub-basin. Each map was selected to highlight the third-order trend of the main four sequences within the Yacoraite Formation Within each of the four sequences, some key periods and/or surfaces (sequence boundary, transgressive trend, maximum flooding surface, regressive trend) were selected to provide an overview of the stratigraphic architecture of the Yacoraite Formation in the Alemania-Metán sub-basin.

During deposition of Sequence 1, the bathymetry of the basin increased, passing from a shallow basin dominated by shallow clastic deposits supplied by the erosion of the rift shoulders and syn-rift deposits (Figure 13A), to a deeper basin with almost no clastic input (except in the western margin) and the occurrence of extended eulittoral deposits with frequent oolitic banks and offshore profundal deposits in the center of the Alemania-Metán sub-basin. The oolitic banks are mainly located along the Guachipas palaeohigh (Figure 13B), in the central part of the basin. Thickness variations (Figure 12) also suggest the influence of inherited structures that were active during the syn-rift phase. The shoreline location was also mainly controlled by previous syn-rift structures. During the deposition of Sequence 1d, the eulittoral facies association with oolitic bank complexes and depositional systems reached their maximum extent (Figure 13C).

Sequence boundary 2 is well-recorded along the basin margins with sedimentary evidence of the reactivation of alluvial depositional systems.

The base of Sequence 2 (Sequence 2a) records a major flooding of the basin. Wave-energy is still recorded by many sedimentary features and the carbonate production remains significant (extended and thick high-energy eulittoral deposits on the eastern part of the basin). However, the development of oolitic bank complexes is very limited, possibly due to an increasing bathymetry that prevented their deposition along the Guachipas palaeohigh (Figure 13D). As for Sequence 1, the shoreline location was mainly controlled by previous syn-rift structures (Las Viboras sill (LV), Figure 13D through F). This step recorded a widening of the basin as well as an increase in the accommodation rate in the central part.

The topmost part of Sequence 2 records a very rapid flooding event characterized by the renewal of clastic sedimentation and the drastic interruption of carbonate production in the entire basin (top of Sequence 2c, Figure 12), just prior to sequence boundary 3 (Figure 13F).

Sequence boundary 3 records a complete desiccation of the lake, with the development and preservation of metre-thick palaeosoils in the center of the basin. Alluvial plain deposits restricted to the main basin depocenter (Sequence 3a, Figure 13G) records a drastic change of the lake dynamic with the predominance of clastic sediments supplied by the erosion of the emerged basin margins. A first transgressive trend is recorded by a backstepping siliciclastic shoreface (equivalent to the Güemes Member; Figure 13H). The western and southern margin are characterized by an increase in the sediment supply with large prograding deltaic packages. Then, following the first major flooding of Sequence 3a characterized by organic-rich deposits within the Yacoraite Formation, the system drastically changed toward the highly alternating lacustrine dynamic that characterizes Sequence 3b (Figure 13I). The topmost part of Sequence 3 is dominated by a thick prograding deltaic package along the western and the southern margins. Along the eastern margin and the gentle slope of the Cachipunco palaeohigh (CH), the carbonate-dominated marginal facies association prograded into the basin (Figure 13I). The maximum extent of the facies belts is very close to those recorded during Sequence 2. The Las Viboras sill had a limited influence on facies belts (LV in Figure 13I).

Sequence boundary 4 (SB4) records another major desiccation event with erosion and exposure along the margins and deposition of restricted mudflat facies association only preserved in the central part of the basin (Figure 13J). The first aggrading to transgressive trend of Sequence 4 (Figure 13K) is mainly preserved in the central part of the basin. As for Sequence 3, the Guachipas palaeohigh (G) seemed to control the facies distribution during this period of time, which is characterized by shallow highly alternating marginal deposits. The topmost part of Sequence 4 is characterized by highstand system tract-like deposits organized in prograding packages (Figure 13l). They recorded a highly alternating base level with deposition of interbedded organic-rich deposits preserved in the central part of the basin. Siliciclastic input also increased in the basin margins during the topmost part of Sequence 4, precluding sequence boundary 5. While the bathymetry progressively decreased during this progradation, the Guachipas palaeohigh (G) seemed to have controlled the facies belts and thicknesses in the central part of the basin (Figure 13L). The basin was then progressively filled up to sequence boundary 5.

6.2 | Factors controlling the depositional system evolution of the Yacoraite Formation

The evolution of depositional profiles and short-term sequences previously presented have been grouped into two end-members at basin scale: (a) a balanced 'perennial'

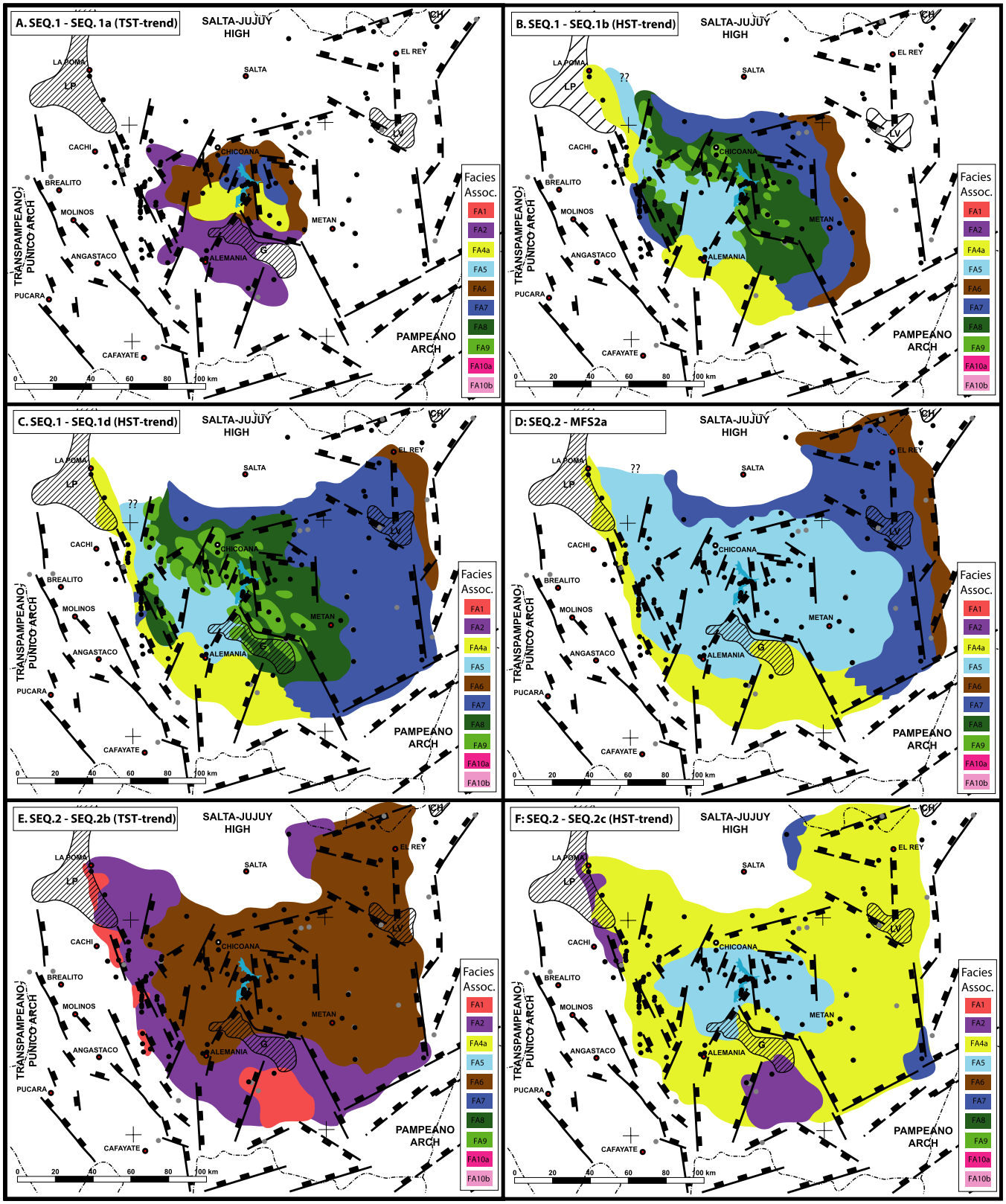

FIGURE 13 Palaeogeographic maps for the Yacoraite Formation in the Alemania-Métan sub-basins. (A) During sequence 1a; (B) during sequence 1b; (C) during sequence 1d; (D) during sequence 2a; (E) during sequence 2b (F) during sequence 2c. Palaeogeographic maps for the Yacoraite Formation in the Alemania-Métan sub-basins. (G) during base sequence 3; (H) during sequence 3a; (I) during sequence 3b; (J) during base sequence 4; (K) during sequence 4a (L) during sequence 4b

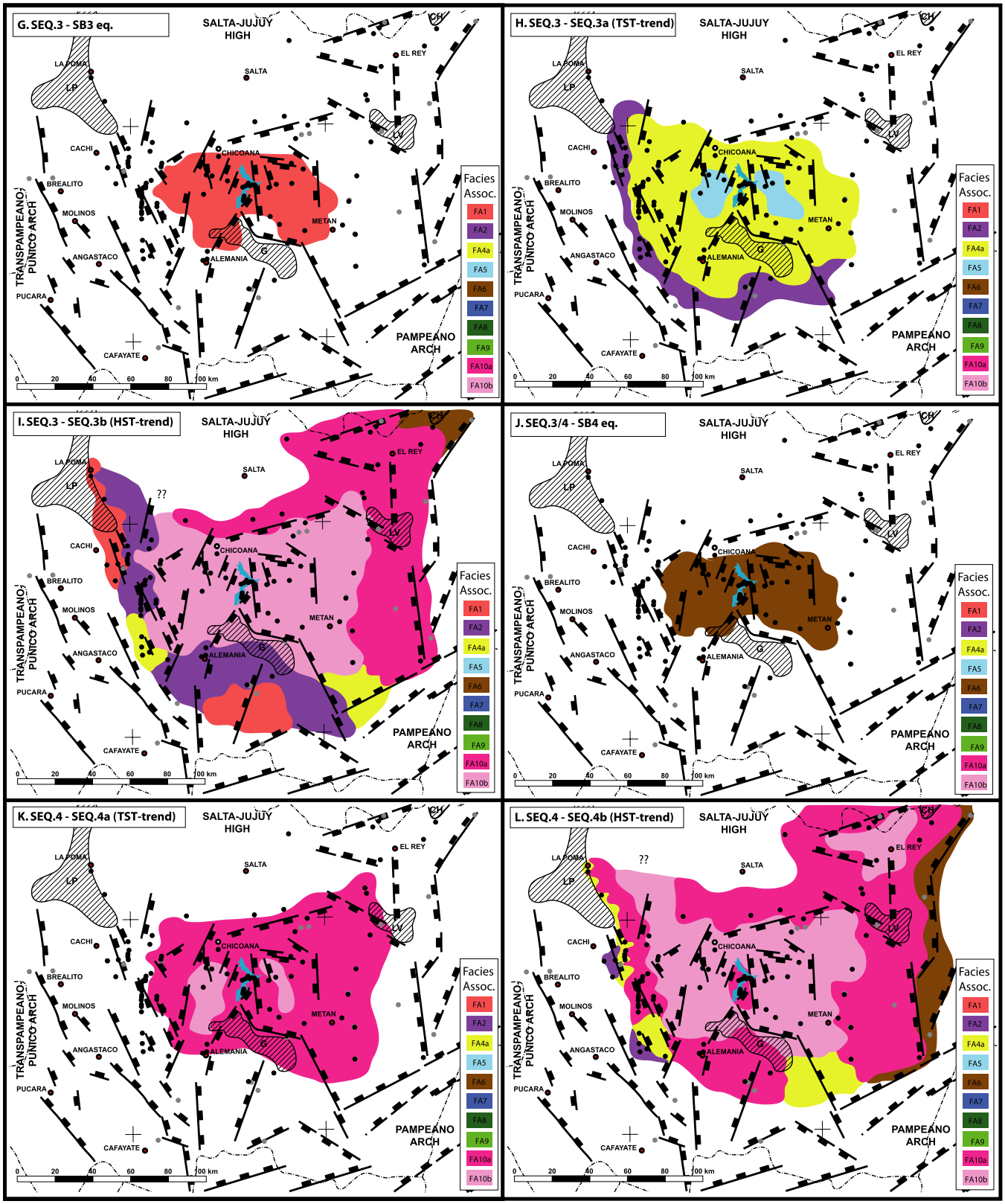

FIGURE 13 Continued

depositional system for the lower part of the Yacoraite Formation (Sequence 1a to Sequence 2b—Amblayo Member), and (b) a highly alternating 'ephemeral' depositional system for the upper part of the Yacoraite Formation (Sequence 2c to Sequence 4b—upper Amblayo to Alemania members). These two depositional models have been considered because the stratigraphic architecture of the Yacoraite Formation indicates a drastic change within the

sedimentary dynamic of the basin (Figure 12) and thus the controlling factors of the sedimentation (tectonic-climate interaction), with a lower part characterized by a relatively stable body of water (high-energy shore deposits, no evidence of full desiccation of the basin), and an upper part characterized by a highly variable body of water (abundant evidence of full desiccation of the basin, relatively low-energy shore). The transition occurred during the deposition of Sequence 2c, with increasing evidence of a full desiccation of the basin.

6.2.1 | Base Yacoraite Formation–Sequence 1a to Sequence 2b

The short-term sequence organization, deposited during the balanced perennial system in the lower part of the Yacoraite Formation (Amblayo Member, as shown in Figure 10), shows four main evolutionary stages (post-sequence boundary, early transgression, maximum transgression and late-regressive) reflecting the relative change of the main controlling factors on lacustrine deposits, represented by the Rainfall (R) / Evaporation (E) ratio (R/E) evolution through time:

- The early stage corresponds to the post-sequence boundary stage, with a low lake level and exposure of the lake margins. During this stage, the system tends to be reactivated with a very low but increasing R/E, and progradation of shallow lacustrine sediments in the basin with a deltaic system and shoreface deposits in the western margin, and eulittoral carbonate deposits in the eastern margin (Figure 14A).
- The early transgression is characterized by a rapid increase of the lake level, accompanied by an active drainage of the basin to the west. The R/E is still low, but increases. The lake-level rise is compensated by the sediment supply, with deposition of aggrading clastic, deltaic and shoreface deposits to the west and high-energy carbonated eulittoral deposits to the east (Figure 14B).
- The maximum transgression (towards the maximum flooding that corresponds to the highest lake level with the maximum expansion) is characterized by an increasing and high R/E. The lake-level increases faster than the sediment supply and retrogradation of the deposits is observed through a backstepping trend of the facies belts (Figure 14C).
- The late regressive stage of the short to mid-term sequences is characterized by high and stable lake levels, with a low stable R/E, which results in the progradation of the facies belts towards the basin center, in a high-energy system. The western margin of the basin is dominated by the deposition of coarse-grained deltaic systems and high-energy shorefaces, whereas the eastern margin is dominated by the progradation of the eulittoral environment (FA8) interbedded with frequent wave-dominated ooid-rich banks (FA9) (Figure 14D).

The short-term sequence organization for the upper part of the Yacoraite Formation (e.g. Top Amblayo, Güemes and Alemania members) shows a drastically different pattern from the lower part of the Amblayo Member.

6.2.2 | Mid-Yacoraite Formation—Sequence 2c to Sequence 3a

The top of the Amblayo Member sequence organization (Sequence 2C) shows an early stage (post-sequence boundary) characterized by widespread basin mudflat deposits, with exposure of the basin margins, which show evidence of a drastic change into a low-gradient (flat) depositional profile (Figure 14E). These low accommodations and very shallow low-energy deposits are the result of a very low R/E, with a lot of evaporation, likely resulting from an arid climate. The transgressive trend up to the maximum flooding surface (Figure 14F) records a reactivation of the drainage system with shallow water clastic sediments deposited in a shoreface setting throughout the entire basin, giving evidence of a climate humidification trend.

Above, Sequence 3a shows another change in the short-term organization sequence, with complete desiccation of the lake and evidence of soil development in the center of the basin (SB3) (Figure 14G). This highly evaporative stage is followed by a new reactivation of the basin drainage due to an increase in rainfall, and a new transgression marked by shallow clastic deposits supplied by deltaic systems in the western margin of the basin and shoreface deposits towards the center of the basin (Figure 14I).

6.2.3 | Top Yacoraite Formation—Sequence 3b to Sequence 4b

The depositional model for the upper part of the Yacoraite Formation at basin scale (highly alternating lacustrine 'ephemeral' depositional system, Alemania Member) includes three main stages in the short-term sequence development, as displayed in the stratigraphic correlations (Figure 12):

- The early stage is characterized by a very low R/E ratio with evidence of exposure all along the basin. Metre-scale desiccation cracks can be observed in the central part of the basin (Figure 11D), while along the basin margin and in the palaeohigh setting, major erosion occurred. Mud clasts and breccias comprized of stromatolite clasts generally drape the exposure/erosional surface (Figure 9).

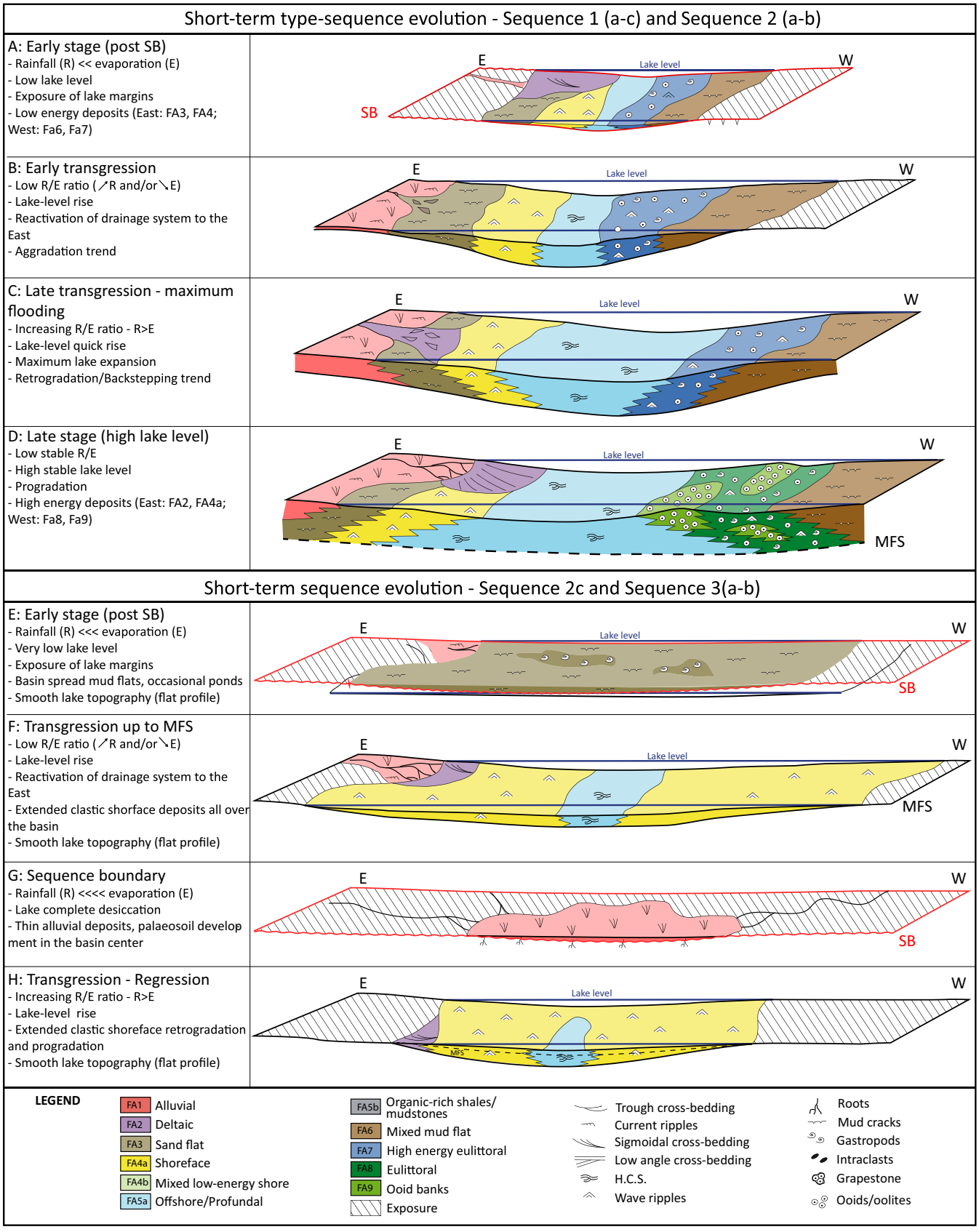

FIGURE 14 Mid-term sequence evolution and conceptual depositional model for the Yacoraite Formation at basin scale. (A) Depositional model for sequences 1 (a-c) and 2 (a-b); (B) Depositional model for the sequences 2d and 3 (a–b)

- The transgressive stage is characterized by an increasing R/E ratio with a backstepping depositional system and major reactivation of the fluvial inputs to the west (Figure 12). Evidence of full desiccation of the basin was documented several times, indicating repetitive high amplitude base-level changes (Figure 9). The body of water recorded an overall bathymetry increase with retrogradation of the alternating marginal facies association towards the basin margins. Organic-rich deposits in Sequence 3b (maximum TOC) were well-preserved in the central part of the basin and are organized in decimetre-scale discontinuous beds.
- The late regressive stage is characterized by a high and highly alternating R/E ratio with aggrading and prograding marginal-alternating facies associations, subdivided into numerous small-scale sequences (Figure 9) that give evidence of a rapid shift between arid conditions with a full or partial desiccation of the system, and humid conditions with reactivation of the basin drainage. This stage also corresponds to the maximum lake encroachment in terms of lake water extent and a reduced lake bathymetry, and may also influence the sensitivity of the system regarding the R/E ratio. The late stage of short-term sequence development of the Alemania Member is characterized by the progradation of the alternating depositional systems.

6.2.4 | Short-term *versus* mid-term sequences

Temperature reconstruction across the K-T boundary, based on a dynoflagelate assemblage analysis (Brinkhuis *et al.*, 1998) and foraminifer stable isotope measurements (Huber *et al.*, 2018), show that the climate at the earth's surface was warm and stable during the latest Maastrichtian, in contrast to strongly fluctuating and cooler conditions during the earliest Danian, similar to the sedimentary record observed in the Salta Basin. Considering the long-term sequence (*ca* 5 Myr), the basin recorded a main subsiding phase between SB1 and MFS2 (Sequence 1 to Sequence 2b), and then an infill phase until SB2c, with mudflats covering the whole basin. Then during Sequence 3a to Sequence 4b, the basin underwent quite a stable low subsidence, and alternating facies (FA10) associations prevailed recording rapid lake-level fluctuations attributed to short-term climate changes with rapid shifts between arid and humid periods until the deposition of the Tunal Formation in an alluvial depositional setting (Figures 9 and 13).

The short-term sequences are mainly controlled by climate–derived parameters, such as rainfall (linked with humidity) and evaporation (linked with aridity). Those two parameters strongly influence, respectively, sediment supply and lake-level variations over time (Dearing, 1997; Wagreich *et al*., 2014).

The response of the depositional system also depends on the tectonic setting through the subsidence pattern, which evolves during the deposition of the Yacoraite Formation, from mechanical to thermal at the transition from syn-rift to sag phase, with low and stable subsidence during the sag phase (Stark, 2011). The tectonic controlling factor is not dominant in terms of short-term sequences (Figure 15), but remains the main driver of the accommodation variation through time. Basal sequences (Sequence 1 to Sequence 2b) are considered to be high accommodation sequences compared to the upper sequences (Sequence 2c to Sequence 4b), with an overall reduced bathymetry that enabled the recording of rapid lake-level fluctuations with frequent complete desiccation and shallow lacustrine deposits during subsequent lake-level rises.

The age model provided by Rohais *et al.* (2019) made it possible to make an initial estimate of the duration of the short-term sequences as well as to discuss the primary controlling factor on the deposition of the short-term and very short-term sequences (Figure 15). The uncertainties regarding the ages given by Rohais *et al.* (2019) are approximately the same as the duration of the cycles given here. The discussion is based on the mean behaviour of the system considering the exact ages given by Rohais *et al.* (2019). It is observed that the overall duration of short-term sequences decreases from Sequence 1a at the bottom up to Sequence 2b. Sequences 1a and 1b last respectively 1.6 and 1Myr, and record the transition from the syn-rift system to the sag phase. It is assumed that these two short-term sequences are mainly tectonically driven. Sequences 1c to 2b are estimated ranges between 0.4 and 0.1 Myr in duration, with a low but increasing sediment supply and an increase in carbonate production (Figure 15; Rohais *et al.*, 2019). These sequences record smoothed short term lake-level variation in a stable low thermal-dominated subsidence (Stark, 2011), potentially forced by earth orbital control, and presumably records the variation of earth eccentricity.

The post-K–T boundary mid-term Sequence 3 duration is estimated at 0.4 Myr, and it is proposed here that this sequence mainly records the variation of the earth eccentricity orbital parameter. Sequence 3 can be subdivided into two short-term sequences (Sequences 3a and 3b), and further subdivided into very short-term cycles (Figure 15), of approximately 0.06 Myr in duration, that could be dominantly attributed to earth obliquity variations, which are recorded in the highly alternating sedimentary deposits.

Sequences 4a and 4b last respectively 0.4 and 0.55 Myr, and their deposition is also supposed to be mainly controlled by earth eccentricity variations. Very short-term sequences can also be identified within Sequences 4a and 4b, with a duration of about 0.1 Myr, that also corresponds to eccentricity periods of about 0.1 Myr (Figure 15).

Regarding the sequence hierarchy and their durations, most of the short-term sequences are climate-driven, controlled by

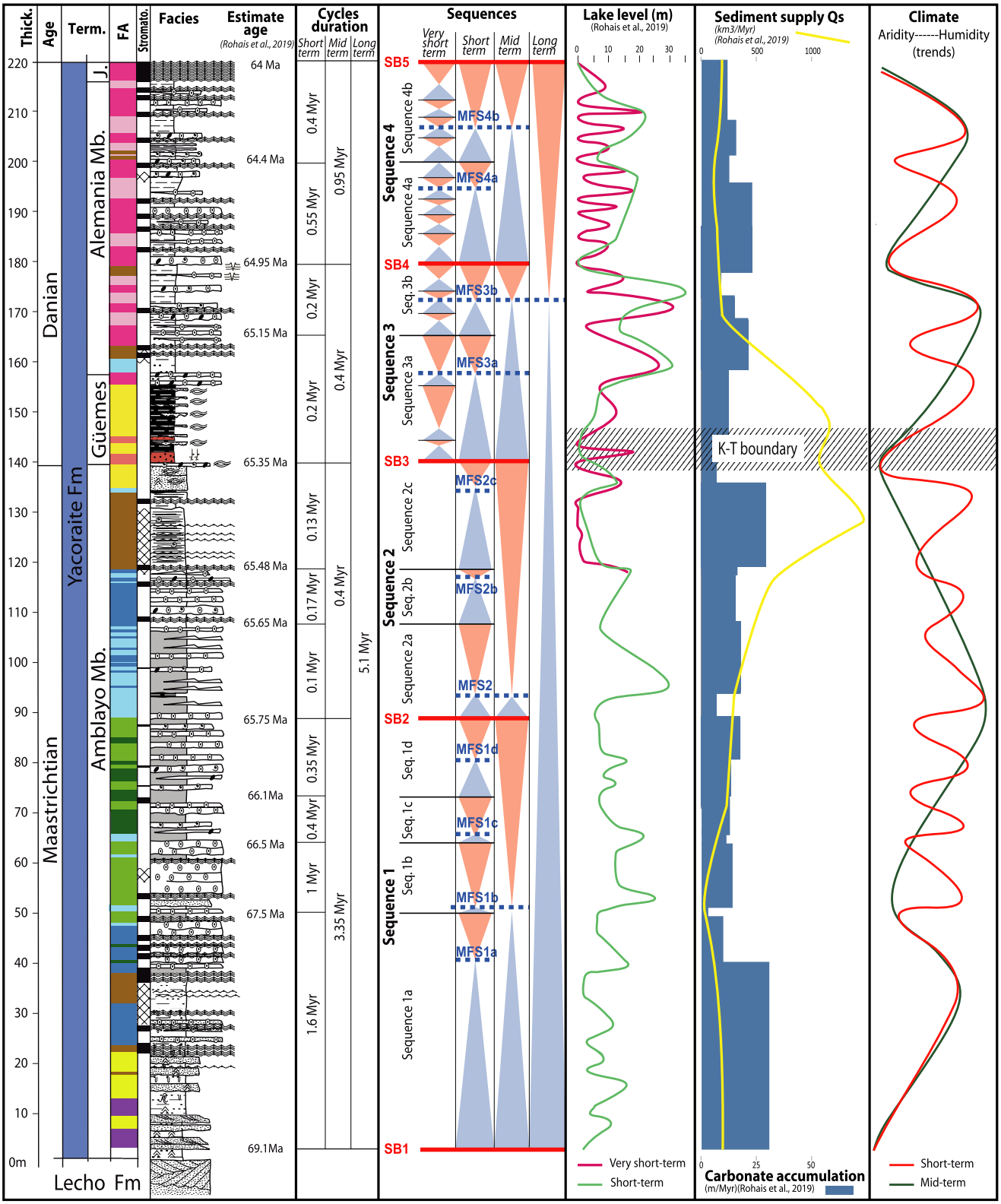

FIGURE 15 Reference section for the Yacoraite Formation in the Alemania and Metan sub-basins (Cabra Corral area) with sequence interpretation, age model (from Rohais *et al.*, 2019) and lake-level variations

earth eccentricity variations, except for the basal Sequences 1a and 1b, that are likely to be mainly controlled tectonically, during the early stage of the sag phase. Sequence 3, deposited just after the K–T event, records both eccentricity with short-term sequences and obliquity variations with the very short-term sequences subdivision. The Sequence 4 succession records

mainly the earth eccentricity variations using periods of 0.1 Myr for very short-term cycles, and periods of about 0.4 Myr for the short-term sequences. The climate variations inducing lake-level variations are interpreted in terms of aridity and humidity trends, as shown in Figure 15. These trends are mainly controlled by earth eccentricity variations on the short-term sequence level, with a combined effect of the obliquity recorded after the K–T boundary. This results in the highly alternating deposits observed at the top of the Yacoraite Formation, with complete desiccation of the lake and subsequent rapid reflooding in a shallow lake system. The system was probably more sensitive to earth orbital parameters during Sequences 3 and 4 because the lake was wider and shallower than in Sequences 1 and 2, and therefore more sensitive to evaporation.

6.3 | Expression of the K-T boundary in the lacustrine sedimentary record

The Yacoraite Formation sedimentary succession encompasses the K/T boundary (*Rohais et al.*, 2019). According to the most recent version of the International Commission for Stratigraphy (Cohen *et al.*, 2013), the K-T boundary is dated at 65.5 Ma, and occurs in the Yacoraite Formation in the Amblayo Member, just below the Güemes Member, at the top of Sequence 2, close to SB3 (Rohais *et al.*, 2019). In the north-western part of the Alemania-Metan Basin, dinosaur tracks have been found at the top of the Amblayo Member, and are considered to be the latest dinosaur tracks found in this area (Díaz-Martínez *et al*., 2017). At this stage of evolution, the lacustrine system was expanding and evolving optimally when climate disturbances occurred and affected the architecture of the Yacoraite deposits.

The K-T boundary is characterized by a drastic climate change, caused by multiple catastrophic events such as multiple meteorite impacts (i.e., Chicxulub crater, Shiva crater; Keller *et al.*, 2004; Chatterjee *et al.*, 2006) and the Deccan Traps flood basalts, that are coeval according to several authors (Duncan and Pyle, 1988; Alvarez, 1997). These events resulted in an immediate and severe short-lived temperature drop at the surface of the earth (Vellekoop *et al.*, 2014) caused by dust blocking the solar radiation. This short-term cooling was then followed by a significant warming due to a substantial release of CO_2, which increased the greenhouse effect.

The sedimentary record of these drastic events can be recognized within the Yacoraite Formation. At the top of Sequence 2 (Sequence 2C, Figures 10 and 12), a blanket of clastic shoreface deposits abruptly overlay eulittoral and mudflat environments (Figure 14E,F), and correspond to a sharp transition from carbonate-dominated deposits to clastic deposits (Figure 14D,E). It is suggested that this change, which corresponds to the shutdown of carbonate production together with an increase of the clastic supply (Figure 15), can be attributed to the K–T event, implying a massive dust cloud and acid aerosols released into the atmosphere (Ocampo *et al.*, 2006). This dust cloud may have blocked the sunlight for a sufficient period of time, resulting in the inhibition of photosynthesis, accounting for the extinction of plants and animals dependent on the light, and thus drastically reducing carbonate production. The re-appearance of siliciclastics in that interval results in an increased supply of sediment coming from the increased erosion of the catchment area, probably eased by the disappearance of soils and vegetation.

Above the siliciclastic blanket at the top of Sequence 2c, SB3 marks a complete desiccation of the lake, followed by a transgressive interval made up of alluvial deposits overlain by clastic shoreface deposits (Figure 14G,H). The complete desiccation of the water mass was supposedly caused by a warm dry period where evaporative processes prevailed over other controlling factors. As stated by many authors (Pope *et al.*, 1997; Piezzaro *et al.*, 1998), the short-term cooling caused by the meteorite impacts and the Deccan Traps was followed by a rapid and significant warming of the atmospheric temperature, higher than the temperatures that prevailed before the K–T event (Vellekoop *et al.*, 2014; Mac Leod *et al.*, 2018). The deposition of a transgressive interval of alluvial and shoreface deposits above SB3 indicates a reactivation of the drainage supplying clastics to the system. This implies a more humid period and a rapid flooding of the system after a warming phase and desiccation of the system.

Above this clastic interval corresponding to the transgressive part of Sequence 3a, the highly alternating lacustrine system was progressively developing, characterized by the abrupt alternation of profundal deposits and marginal carbonate-dominated eulittoral to supralittoral deposits, with a very limited amount of clastics in this depositional system. The carbonate production was again active mostly in the eastern part of the basin (Figure 15), suggesting a resumption of 'normal' conditions, comparable to those prevailing during the deposition of Sequences 1 and 2a-b prior to the K–T event. The onset of this highly alternating, or 'ephemeral' depositional system might be due to the fact that the lake bathymetry is very reduced (according to the stacking of facies associations and the geometries of the lake profiles deduced from stratigraphic correlations), or at least lower during Sequences 3 and 4 than Sequences 1 and 2, permitting a very rapid basinward shift of facies when the lake-level dropped. Unfortunately, this hypothesis cannot be quantified properly with this work as the bathymetric proxies were only based on the ranking of the maximum flooding surfaces through the encroachment of lake deposits on the basin margins. The lack of well-preserved sedimentary

structures associated with wave dynamics in the topmost part of the Yacoraite Formation (Sequences 3 and 4) does not allow the depth of the bodies of water to be estimated (Tanner, 1971).

7 | CONCLUSION

1. The Yacoraite Formation recorded the deposition of siliciclastic and carbonate-dominated deposits in the western and eastern margins, respectively, of the Salta Rift Basin (Alemania-Metán sub-basins) in a lacustrine environment. The Yacoraite Formation encompasses 10 facies associations organized according to deposition energy, and the vicinity of the clastic sources.
2. The Yacoraite Formation recorded the complete life cycle, from the early sag phase to the late rifting phase. The basal sequences record a perennial lake system (Sequences 1 and 2). Above, the sequences are characterized by an ephemeral highly alternating depositional system (Sequences 3 and 4).
3. The Yacoraite Formation is organized into four mid-term sequences in an overall long-term order sequence, 5 Myr in duration. The mid-term sequences can be subdivided into higher order sequences (short-term sequences, *ca* 100–250 Myr each) recording mainly high frequency climate variations.
4. The occurrence of various depositional sequences in the Yacoraite Formation primarily reflects the variations of the Rainfall/ Evaporation ratio, leading to prograding, retrograding or aggrading trends in a stable lake system (lower sequences) and a highly alternating lake system (upper sequences). In that sense, the Yacoraite Formation can be considered a textbook example of sequence stratigraphy in a lacustrine setting. In this study, it is possible to identify and characterize the stacking of the different short to mid-term sequences at basin scale, which would not have been possible without this overall view of the Alemania-Metán sub-basins.
5. The Yacoraite Formation is dated at Maastrichtian-Danian. The K–T event is recorded within the Yacoraite Formation, at the transition between the 'perennial' stable lake system and the 'ephemeral' highly alternating system. This transition is characterized by a widespread siliciclastic interval, as well as a lack of carbonate deposits, in which the first major evidence of complete desiccation of the lake can be observed.
6. Short-term variations in the sedimentary record were mainly forced by eccentricity. Very short-term variations are however recognized in the post-K–T boundary deposits, representing very high frequency cycles with highly alternating deposits controlled by earth eccentricity variations modulated by obliquity variations.

ACKNOWLEDGEMENT

Part of this work was supported by companies in the frame of the Joint Industrial Project COMPAS leaded by IFP Energies nouvelles: BHP Billiton, BP, Chevron, Cobalt Inc., Ecopetrol, ENI, ExxonMobil, GalpEnergia, Total, MaerskOil, Petrobras, Repsol, YPF S.A. We would like to thank Claudia Galli and José Salfity for their help and support during the initiation of this study in the Salta-Jujuy provinces. We also acknowledge the two anonymous reviewers and the editors that helped at greatly improve the manuscript. The authors of this manuscript declare that there is no conflict of interest.

DATA AVAILABILITY

Data available on request from the authors. The data that support the findings of this study are available from the corresponding author upon reasonable request.

ORCID

Rémy Deschamps https://orcid.org/0000-0002-0888-3456
Sébastien Rohais https://orcid.org/0000-0002-0659-4714
Youri Hamon https://orcid.org/0000-0003-4794-0254
Marta Gasparrini https://orcid.org/0000-0003-3438-4922

REFERENCES

Alonso, R.N. and Marquillas, R.A. (1986) Nueva localidad con huellas de dinosaurios y primer hallazgo de huellas de aves en la Formacion Yacoraite (Maastrichtiano) del Norte Argentino. Actas 4th Congress Arg Paleont Bioestrat, 2, 33–41.

Alonso Zarza, A.M. and Tanner, L.H. (2009) *Carbonates in Continental Settings: Geochemistry, Diagenesis and Applications*. Elsevier.

Alvarez, W. (1997). T. rex and the Crater of Doom. Princeton University Press. pp. 130–146. ISBN 978-0-691-01630-6.

Arp, G. (1995) Lacustrine bioherms, spring mounds, and marginal carbonates of the Ries-Impactcrater (Miocene, Southern Germany). *Facies*, *33*, 35–90.

Bento Freire, E. (2012) Caracterização estratigráfica em alta resolução das sequências calcarias de origem microbiana do intervalo paleocênico da Formação Yacoraite (Sequência Balbuena IV) na região de Salta – Argentina. Thesis (Master). Curso de Geologia, Instituto de Geociências, Universidade Federal do Rio de Janeiro, Rio de Janeiro, 243 pp.

Blair, C. and Bilodeau, W.L. (1988) Develpment of tectonic cyclothems in rift, pull apart, and foreland basins: sedimentary response to episodic tectonism. *Geology*, *16*(1988), 517–520.

Bohacs, K.M., Carroll, A.R. and Neal, J.E. (2003) Lessons from large lake systems – thresholds, nonlinearity, and strange attractors. *Geological Society of America Special Paper*, *370*, 2003.

Bohacs, K.M., Carroll, A.R., Neal, J.E. and Mankiewicz, P.J. (2000) Lake-basin type, source potential, and hydrocarbon character: an integrated-sequence-stratigraphic– geochemical framework. In:Gierlowski-Kordesch, E.H. and Kelts, K.R. (Eds.) *Lake Basins through Space and Time*. *AAPG Studies in Geology*, *46*, 3–34.

Bonaparte, J.F. and Bossi, G.E. (1967) Sobre la presencia de dinosaurios en la Formacion Pirgua del rupo Salta y su significado cronologico. *Acta Geologica Lilloana*, *9*, 25–44.

Bossi, G.E. (1969) Geología y estratigrafía del sector sur del valle de Choromoro. *Acta Geologica Lilloana*, *10*, 17–64.

Brinkhuis, H., Bujak, J.P., Smit, J., Versteegh, G.J.M. and Visscher, H. (1998) Dinoflagellate-based sea surface temperature reconstructions across the Cretaceous-Tertiary boundary. *Palaeogeography, Palaeoclimatology, Palaeoecology*, *141*(1998), 67–83.

Bunevich, R., Borghi, L., Gabaglia, G.P.R., Terra, G.J.S., Bento Freire, E., Lykawka, R. *et al*. (2017) Microbialitos da Sequência Balbuena IV (Daniano), Bacia de Salta, Argentina: caracterização de intrabioarquiteturas e de microciclos. *Pesquisas em Geociencias*, *44*(2), 177–202.

Camoin, G., Casanova, J., Rouchy, J.-M., Blanc-Valleron, M.-M. and Deconinck, J.-F. (1997) Environmental controls on perennial and ephemeral carbonate lakes: the central palaeo-Andean Basin of Bolivia during Late Cretaceous to early Tertiary times. *Sedimentary Geology*, *113*, 1–26.

Carrera, N., Munoz, J.A., Sabat, F., Roca, E. and Mon, R. (2006) The role of inversion tectonics in the structure of the Cordillera Oriental (Argentinean Andes). *Journal of Structural Geology*, *28*, 1921–1932.

Carrera, N., Muñoz, J.A. and Roca, E. (2009) 3D reconstruction of geological surfaces by the equivalent dip-domain method: an example from field data of the Cerro Bayo Anticline (Cordillera Oriental, NW Argentine Andes). *Journal of Structural Geology*, *31*, 1573–1585.

Chatterjee, S., Guven, N., Yoshinobu, A. and Donofrio, R. (2006). Shiva structure: a possible KT boundaryimpact crater on the western shelf of India. Special publication of the Museum of Texas Tech University (50).

Chuanmao, L., Friedman, G.M. and Zhaochang, Z. (1993) Carbonate storm deposits (tempestites) of Middle to Upper Cambria nage in the Helan mountain, northwest China. *Carbonates and Evaporites*, *8*, 181. https://doi.org/10.1007/BF03175176

Clausing, A. (1990) Mikrofazies lakustriner Karbonat-horizonte des Saar-Nahe-Beckens (Unterperm, Rotliegend, SW-Deutschland). *Facies*, *23*, 121–140.

Clebsch, C.A. (1991) The geological evolution of the Paraguayan Chaco. PhD Thesis, Texas Tech University.

Cloetingh, S., McQueen, H. and Lambeck, K. (1985) On a tectonic mechanism for regional sealevel variations. *Earth and Planetary Science Letters*, *75*, 157–166.

Cohen, K.M., Finney, S.C., Gibbard, P.L. and Fan, J.X. (2013) The ICS international chronostratigraphic chart. *Episodes*, *36*, 199–204.

Contreras, J., Scholz, C.H. and King, G.C.P. (1997) A general model of rift basin evolution: constraints of first order stratigraphic observations. *Journal of Geophysical Research*, *102*, 7673–7690.

Cristallini, E., Comınguez, A.H. and Ramos, V.A. (1998) Deep structure of the Métan-Guachipas region: Tectonic inversion in Northwestern Argentina. *Journal of South American Earth Sciences*, *10*, 403–421.

Dalrymple, R.W. (2010) Tidal depositional systems. In: James, N.P. and Dalrymple, R.W. (Eds.), *Facies Models 4*. St. John′s: Geological Association of Canada, pp. 201–232.

De Wet, C.B., Yocum, D.A. and Mora, C.I. (1998) Carbonate lakes in closed basins: sensitive indicators of climate and tectonics; an example from the Gettysburg Basin (Triassic), Pennsylvania. *USA Special Publications*, *59*(1998), 191–209.

Dearing, J.A. (1997) Sedimentary indicators of lake level changes in humid temperate zone: a critical review. *Journal of Paleolimnology*, *18*(1–14), 1997.

Díaz-Martínez, I., González, S. and de Valais, S. (2017) Dinosaur footprints in the Early Jurassic of Patagonia (Marifil Volcanic Complex, Argentina): biochronological and palaeobiogeographical inferences. *Geological Magazine*, *154*(4), 914–922. https://doi.org/10.1017/S0016756817000103

Dickson, J.A.D. (1966) Carbonate identification and genesis as revealed by staining. *Journal of Sedimentary Petrology*, *36*(2), 491–505.

Dukle, W.L. (1985) Hummocky cross-stratification, tropical hurricanes, and intense winter storms. *Sedimentology*, *32*, 167–194.

Duncan, R.A. and Pyle, D.G. (1988) Rapide eruption of the Deccan flood basalts at the Cretaceous/Tertiary boundary. *Nature*, *333*, 841–843.

Dunham, R.J. (1962). Classification of Carbonate Rocks according to depositional texture. In: Ham, W.E. (Ed.) *Classification of Carbonate Rocks*. *AAPG Memoir*, *1*, 108–121.

Eardley, A.J. (1966) Sediments of the Great Salt Lake. Guidebook Geology of Utah, 20, Utah Geological Society, pp. 105–120.

Fernandez, J. (1975) Hallazgo de peces pulmonados fosiles en la Puna Jujena. *Anales de la Sociedad Cientifica Argentina*, *2*(41), 13–18.

Flügel, E. (2004) *Microfacies of carbonate rocks. Analysis, interpretation and application*. Berlin: Springer, 976 p.

Galliski, M.A. and Viramonte, J.G. (1988) The Cretaceous paleorift in northwestern Argentina: A petrologic approach. *Journal of South American Earth Sciences*, *1*, 329–342.

Galloway, W.E. (1975) Process framework for describing the morphologic and stratigraphic evolution of deltaic depositional systems. In: Broussard, M.L. (Ed.) *Deltas, Models of Exploration*. Houston, TX: Houston Geological Society, pp. 87–98.

Gomes, P.O., Kilsdonsk, B., Minken, J., Grow, T. and Barragan, R. (2009) The outer high of the Santos basin, southern Sao Paulo plateau, Brazil: Pre-Salt exploration outbreak, paleogeographic settings and evolution of the syn-rift structures. American association of Petroleum Geologists Cape Town Conference, search and discovery article no. 10193.

Gómez-Omil, R.J., Boll, A. and Hernández, R.M. (1987) Cuenca cretácico-terciaria del Noroeste argentino (Grupo Salta). In: X Congr. Geol. Argent., 5, Tucumán, p. 9 (inédit).

Gwynn, J.W. and Murphy, E.J. (1980) Recent sediments of the Great Salt Lake basin. *Utah Geological and Mineral Survey Bulletin 116*, 83–96.

Hardie, L.A., Smoot, J.P. and Eugster, H.P. (1978) Saline lakes and their deposits. A sedimentological approach. In: Matter, A. and Tucker, M. (Eds.) *Modern and Ancient Lake Sediments*, vol. 2. IAS Special Publication, pp. 7–41.

Huber, B.T., MacLeod, K.G., Watkins, D.K. and Coffin, M.F. (2018) The rise and fall of the Cretaceous hot greenhouse climate. *Global and Planetary Change*, *167*(2018), 1–23.

Keller, G., Adatte, T., Stinnesbeck, W., Rebolledo, V., Fucugauchi, J.U., Kramar, U. *et al*. (2004) Chicxulub impact predates the K-T boundary mass extinction. *PNAS*, *101*, 3753–3758.

Kring, D.A. (2003) Environmental consequences of impact cratering events as a function of ambient conditions on Earth. *Astrobiology*, *3*(1), 133–152.

Lambiase, J.J. and Bosworth, W. (1995) Structural controls on sedimentation in continental rifts. In Lambiase, J.J. (Ed.) *Hydrocarbon habitat in rift basins*. *Geological Society Special Publication*, *80*, 117–144.

Lin, C.S., Eriksson, K. and Li, S.T. (2001) Sequence architecture, depositional systems, and controls on development of lacustrine basin fills in part of the Erlian Basin, Northeast China. *AAPG Bulletin*, *85*, 2017–2043.

MacLeod, K.G., Quiton, P.C., Sepúlveda, J. and Negra, M.H. (2018) Postimpact earliest Paleogene warming shown by fish debris oxygen isotopes (El Kef, Tunisia). *Science*, *360*(6396), 1467–1469.

Mädel, F. (1984) Estratigrafıa del tramo inferior del pozo descubridor Palmar Largo x–1. *Bol. Inform. Petrol.*, *1*(2), 109.

Marquilla, M.A., Salfity, J.A., Matthews, S.J., Matteini, M. and Dantas, E.L. (2011) U-Pb zircon age of the Yacoraite Formation and its significance to the Cretaceous-Tertiary boundary in the Salta Basin, Argentina. *Cenozoic Geology of the Central Andes of Argentina*, *227–246*, 2011/227.

Marquillas, R.A. (1985) Estratigrafıa, sedimentologıa y paleoambientes de la Formacion Yacoraite (Cretacico Superior) en el tramo austral de la cuenca, norte argentino. Tesis Doctoral, Universidad Nacional de Salta, pp. 1–139.

Marquillas, R.A., del Papa, C.E. and Sabino, I.F. (2005) Sedimentary aspects and paleoenvironmental evolution of a rift basin: Salta group (Cretaceous–Paleogene), northwestern Argentina. *International Journal of Earth Sciences*, *54*, 94–113.

Marquillas, R.A., Sabino, I.F., Sial, A.N., Del Papa, C., Ferreira, V. and Matthews, S. (2007) Carbon and oxygen isotopes of Maastrichtian-Danian shallow marine carbonates: Yacoraite Formation, northwestern Argentina. *Journal of South American Earth Sciences*, *23*, 304–320.

Moreno, J.A. (1970) Estratigrafıa y paleogeografıa del Cretacico superior en la cuenca del noroeste argentino, con especial mencion de los Subgrupos Balbuena y Santa Barbara. *Revista de la Asociación Geológica Argentina*, *24*, 9–44.

Moroni, A.M. (1982) Correlacion palinologica en las Formaciones Olmedo y Yacoraite. Cuenca del Noroeste Argentino, 3rd Congr edition. Geol Chil, pp. 340–349.

Ocampo, A., Vajda, V. and Buffetaut, E. (2006) 'Unravelling the Cretaceous-Paleogene (KT) catastrophe: Evidence from flora fauna and geology. In: Cockell, C., Gilmour & Koelberl, C. (Eds.) *Biological Processes Associated with Impact Events*. Berlin: Springer, pp. 197–219.

Omarini, R.H., Salfity, J.A., Linares, E., Viramonte, J.G. and Gorustovich, S.A. (1989) Petrologia geoquimica y edad de un filon lamproitico en el Subgrupo Pirgua (Alemania-Salta). Revista del Instituto de Geologia y Mineria 7 (Universidad Nacional de Jujuy).

Picarelli, A. and Abreu, V. (2012). Sequence Stratigraphy Applied to Continental Rift Basins: Example from Recôncavo Basin, Brazil. In Baganz, O.W., Bartov, Y., Bohacs, K. and Nummedal, D. (Eds.) *Lacustrine sandstone reservoirs and hydrocarbon systems*. *AAPG Memoir*, *95*, 347–366.

Pierazzo, E., Kring, D.A. and Melosh, H.J. (1998) Hydrocode simulation of the Chicxulub impact event and the production of climatically active gases. *Journal of Geophysical Research*, *103*(E12), 28607–28625.

Pietras, J.T. and Carroll, A.R. (2006) High-resolution stratigraphy of an under filled lake basin: Wilkins Peak Member, EoceneGreen River Formation, Wyoming. *Journal of Sedimentary Research*, *76*, 1197–1214.

Platt, N.H. and Wright, V.P. (1991) Lacustrine carbonates: facies models, facies distributions and hydrocarbon aspects. In: Anadon, P., Cabrera, L. and Kelts, K. (Eds) *Lacustrine Facies Analysis*. *IAS Special Publications*, *13*, 57–74.

Pope, K.O., Baines, K.H., Ocampo, A.C. and Ivanov, B.A. (1997) Energy, volatile productions, and climatic effects of the Chicxulub Cretaceous-Tertiary impact. *Journal of Geophysical Research*, *102*(E9), 21645–21664.

Powell, J.E. (1979) Sobre la presencia de dinosaurios y otras evidencias de vertebrados del Cretacico superior de la region de La Candelaria, Prov. de Salta, Argentina. *Ameghiniana*, *16*, 191–204.

Quattrocchio, M. and del Papa, C.E. (2000) Paleoambiente de la Secuencia Maız Gordo (Paleoceno Tardıo-Eoceno Temprano), arroyo Las Tortugas, Cuenca del Grupo Salta (NO Argentina). *Palinologıa y Sedimentologıa. Rev Espanola Paleont*, *15*, 57–70.

Quattrocchio, M., Ruiz, L. and Volkheimer, W. (2000) Palynological zonation of the Paleogene of the Colorado and Salta Group basin, Argentina. *Rev Espanola Micropaleont*, *32*, 61–78.

Rangel, H.D. and Carminatti, M. (2000) Rift lake stratigraphy of the Lagoa Feia formation, Campos basin, Brazil, Lake basins through space and time. *American Association of Petroleum Geologists Studies in Geology*, *46*, 225–244.

Reyes, F.C. (1972) Correlaciones en el Cretacico de la cuenca Andina de Bolivia, Peru y Chile. *Rev Tec YPFB*, *1*, 101–144.

Reyes, F.C. and Salfity, J.A. (1973) Consideraciones sobre la estratigrafıa del Cretacico (Subgrupo Pirgua) del noroeste argentino. Actas 5th Congr GeolArg*3*, 355–385.

Reyes, F.C., Salfity, J.A., Viramonte, J.G. and Gutierrez, W. (1976) Consideraciones sobre el vulcanismo del Subgrupo Pirgua (Cretacico) en el norte argentino. Actas 6th Congress Geol Arg, *1*, 205–223.

Roemers-Oliveira, E., Fernandes, L.A., Bento Freire, E. and Simoes, L.S.A. (2015) Filamentos microbianos em estromatólitos e laminitos da Sequência Balbuena III (Maastrichtiano/Daniano) da Formação Yacoraite na Sub-bacia Metán-Alemania, na região de Salta, Argentina, e seus significados paleoambientais. *Brazilian Journal of Geology*, *45*(3), 399–413.

Rohais, S., Hamon, Y., Deschamps, R., Beaumont, V., Gasparrini, M., Pillot, D. *et al*. (2019) Patterns of organic carbon enrichment in a lacustrine system across the K-T boundary: insight from a multi-proxy analysis of the Yacoraite Formation, Salta rift basin, Argentina. *Journal of Coal Geology*, *210*. ISSN, 0166-5162. https://doi.org/10.1016/j.coal.2019.05.015

Salfity, J.A. (1982) Evolucion paleogeogra fica del Grupo Salta (Cretacico-Eogenico), Argentina. Actas 5th Congr Latinoam Geol,Buenos Aires, *1*, 11–26.

Salfity, J.A. and Marquillas, R.A. (1994) Tectonic and sedimentary evolution of the Cretaceous-Eocene Salta Group Basin, Argentina. In: Salfity, J.A. (Ed.) *Cretaceous tectonics of the Andes*. Vieweg and Sohn: Earth Evolution Sciences, Friedr, pp. 266–315.

Scherer, C.M.S., Goldberg, K. and Bardola, T. (2015) Facies architecture and sequence stratigraphy of an early post-rift fluvial succession, Aptian Barbahla Formation, Araripe Basin, northeastern Brazil. *Sedimentary Geology*, *322*, 43–62.

Schulte, P., Alegret, L., Arenillas, I., Arz, J.A., Barton, P.J., Bown, P.R. *et al*. (2010) The Chicxulub asteroid impact and mass extinction at the Cretaceous-Paleogene boundary. *Science*, *327*(5970), 1214–1218.

Seranne, M. and Anka, Z. (2005) South Atlantic continental margins: A comparison of the tectonic vs climate interplay on the evolution of equatorial West Africa and SW Africa margins. *Journal of African Earth Sciences*, *43*(1–3), 283–300.

Shanley, K.W. and McCabe, P.J. (1994) Perspective on the sequence stratigraphy of continental strata. *American Association of Petroleum Geologists Bulletin*, *78*, 544–568.

Starck, D. (2011) Cuenca Cretácica-Paleogena del Noroeste Argentino. 8° Congreso de Exploración y Desarrollo de Hidrocarburos. Visión Actual, Instituto Argentino del Petróleo y el Gas: Simposio Cuencas Argentinas, pp. 407–453.

Tanner, W.F. (1971) Numerical estimates of ancient waves, water depth and fetch. *Sedimentology*, *18*, 71–88.

Uliana, M.A., Biddle, K.T. and Cerdan, J. (1989) Mesozoic extension and the formation of Argentine sedimentary basins. In Tankard, A.J. and Balkwill, H.R. (Eds.) *Extensional tectonics and stratigraphy of the North Atlantic margins*. *AAPG Memoir*, *46*, 599–614.

Valencio, D.A., Giudice, A., Mendıa, J.E. and Oliver, G.J. (1976) Paleomagnetismo y edades K/Ar del Subgrupo Pirgua, provincia de Salta, Republica Argentina. Actas 6th Congr Geol. Arg, 1, 527–542.

Vellekoop, J., Sluijs, A., Smit, J., Shouten, S., Weijers, J.W., Sinninghe Damsté, J.S. *et al*. (2014) Rapide short-term cooling following the Chicxulub impact at the Cretaceous-Paleogene boundary. *PNAS*, *111*(21), 7537–7541.

Viramontes, J.G., Kay, S.M., Becchio, R., Escayola, M. and Novitski, I. (1999) Cretaceous rift related magmatism in central-western South America. *Journal of South-American Earth Sciences*, *12*, 109–121.

Wagreich, M., Lein, R., Sames, B. (2014) Eustasy, its controlling factors, and the limno-eustatic hypothesis – concepts inspired by Eduard Suess. *Austrian Journal of Earth Sciences*, *107*(1), 115–131.

Williamson, C.R. and Picard, M.D. (1974) Petrology of carbonate rocks of the Green River Formation (Eocene). *Journal of Sedimentary Petrology*, *44*(3), 738–759.

Zhang, G., Buatois, L.A., Mangano, M.G. and Acenolaza, F.G. (1998) Sedimentary facies and environmental ichnology of a Permian playa-lake complex in western Argentina. *Paleogeography, Paleoclimatology, Paleoecology*, *138*, 221–243.

SUPPORTING INFORMATION

Additional supporting information may be found online in the Supporting Information section.

How to cite this article: Deschamps R, Rohais S, Hamon Y, Gasparrini M. Dynamic of a lacustrine sedimentary system during late rifting at the Cretaceous–Palaeocene transition: Example of the Yacoraite Formation, Salta Basin, Argentina. *Depositional Rec*. 2020;00:1–33. https://doi.org/10.1002/dep2.116